Adaptive T cells regulate disease tolerance in human malaria

Diana Muñoz Sandoval,[1,2] Florian Bach,[1*] Wiebke Nahrendorf,[1*] Alasdair Ivens,[1,3] Michalina Mazurczyk,[4] Yrene Themistocleous,[5] Sarah E. Silk,[5] Jordan R. Barrett,[5] Nick J. Edwards,[5] Giorgio Napolitani,[4] Angela M. Minassian,[5] Simon J. Draper[5] and Philip J. Spence[1,3]

[1]Institute of Immunology and Infection Research, University of Edinburgh, UK.
[2]Instituto de Microbiologia, Universidad San Francisco de Quito, Ecuador.
[3]Centre for Immunity, Infection and Evolution, University of Edinburgh, UK.
[4]MRC Human Immunology Unit, Weatherall Institute of Molecular Medicine, University of Oxford, UK.
[5]The Jenner Institute, University of Oxford, UK.

* these authors contributed equally
correspondence: philip.spence@ed.ac.uk

impact statement | malaria attenuates T cell activation to increase host fitness

Abstract

Immunity to severe malaria is acquired quickly, operates independently of pathogen load and represents a highly effective form of disease tolerance. The mechanism that underpins tolerance in human malaria remains unknown. We developed a re-challenge model of falciparum malaria in which healthy naive adult volunteers were infected three times over a 12-month period to track the development of disease tolerance in real-time. We found that parasitaemia triggered a hardwired emergency myeloid response that led to systemic inflammation, pyrexia and hallmark symptoms of clinical malaria across the first three infections of life. In contrast, $CD4^+$ T cell activation was quickly modified to reduce the number and diversity of effector cells upon re-challenge. Crucially, this did not silence critical helper T cell functions but instead prevented the generation of cytotoxic effectors associated with autoinflammatory disease. Tolerised hosts were thus able to prevent collateral tissue damage and injury. Host control of T cell activation can therefore be established after a single infection and in the absence of anti-parasite immunity. And furthermore, this rapid host adaptation can protect vital organs to minimise the harm caused by systemic inflammation and sequestration.

Introduction

The epidemiology of human malaria clearly shows that immunity develops in two distinct phases. First, individuals acquire protection against severe life-threatening disease and in areas of high transmission this occurs very quickly (often before 12-months of age) (1-4). Then after many years of exposure protection against clinical malaria is established, which promotes the transition to asymptomatic infection (usually in adolescence) (5). This temporal dissociation between clinical immunity and immunity to severe malaria has led to the assumption that they must be underpinned by different mechanisms of host defense. In agreement, clinical immunity coincides with control of parasite burden (and is therefore supported by mechanisms of host resistance) whereas immunity to severe malaria is acquired independently of pathogen load and is a form of disease tolerance (1). One leading hypothesis suggests that broadly neutralising antibodies that recognise variant surface antigens associated with severe malaria (such as group A/DC8 PfEMP1) could prevent severe disease without affecting total pathogen load (2). In this scenario, immunity to severe malaria would depend upon the rapid production of antibodies that can specifically eliminate pathogenic variants. At present, there is limited evidence that such broad cross-reactivity can be achieved or that neutralising antibodies can be produced within the first year of life to inhibit cytoadherence and reduce sequestration *in vivo* (6). The mechanism that underpins disease tolerance in human malaria therefore remains unclear.

An alternative explanation is that the host response to infection is quickly modified to minimise the harm caused by malaria parasites. It is well known that metabolic adaptations are induced during the blood cycle to increase host fitness (7-9) and control of inflammation might provide an additional path towards disease tolerance (10). In support of this argument, inflammation can be uncoupled from parasite density in children (11) and pathogenic immune responses can be silenced to minimise tissue stress and toxicity in mice (12). Importantly, host control of inflammation as a defense strategy would not rule out a role for variant surface antigens in severe disease. After all, systemic inflammation, tissue damage and hypoxia could create the right conditions for endothelium activation and the selection of pathogenic variants (13). As such, reducing inflammation may minimise the preferential expansion of parasites associated with severe malaria - this would represent a highly effective route to disease tolerance that would not be influenced by parasite strain or genotype.

Host adaptations that are quickly established to reduce disease severity will be hard to identify in an endemic setting due to the difficulty of pinpointing an infant's first infection of life. On the other hand, controlled human malaria infection (CHMI) (14) offers an unparalleled opportunity to investigate mechanisms of disease tolerance. Naive volunteers are inoculated with live and non-attenuated parasites and their response can be tracked throughout infection and convalescence by repeated sampling; pre-infection samples can be collected to provide all-important baseline measurements; and the immune system is exposed to an enormous antigen load at the peak of infection (more than 10^7 parasites per litre of blood) (13). Crucially, adults are more susceptible to severe malaria than children during a first-in-life infection (15, 16) and so we can study the most at-risk group of individuals. We therefore developed a human re-challenge model of falciparum malaria to track the development of disease tolerance in real-time across the first three infections of life.

Results

Malaria does not induce fast-acting mechanisms of host resistance

We developed a human re-challenge model of falciparum malaria in which ten healthy adult volunteers were infected two times (4-months apart) by intravenous injection of infected red cells; six volunteers returned for a third infection 8-months later (figure 1A). A blood challenge model was chosen because it standardises the infectious dose, prolongs the period of blood-stage infection (cf. mosquito challenge) and removes liver-stage immunity as a possible confounding factor upon re-challenge (17, 18). Furthermore, volunteers were always inoculated with the same clonal malaria parasite (3D7) to remove parasite genotype as an infection-dependent variable. Importantly, we used a recently mosquito-transmitted line (< 3 blood cycles from liver egress) (19) since mosquitoes have been shown to reset parasite virulence (20). Volunteers attended clinic the day before infection (baseline), every 12-hours from the day after infection until diagnosis (peak of infection) and then 24- and 48-hours after drug treatment. These frequent visits allowed for regular blood sampling to construct a detailed longitudinal time-course of each volunteer's response to the first three infections of life.

We found that pathogen load and the parasite multiplication rate were comparable between the first, second and third malaria episode (figure 1B-C and supplementary file 1). Whilst epidemiology has shown that anti-parasite immunity does not develop within this time-frame (1) these data nevertheless derive from an endemic setting where each infection is caused by a new parasite genotype. It is remarkable then that in our study (which removes polymorphism as an obstacle to immunity) we find no evidence that volunteers can limit the replication of parasites they have seen previously. Epidemiology has also shown that immunity to clinical malaria is slow to develop, and in most cases is not acquired until adolescence (5). In agreement, we found no significant difference in the number or severity of adverse events (such as headache, fever and fatigue) between first, second and third infection (figure 1D-E). Differential blood counts revealed other hallmark symptoms of clinical malaria, such as lymphopenia and anaemia, were also comparable between infections (figure 1F and figure 1 - supplement 1). These data thus show that healthy adult volunteers do not acquire mechanisms of resistance (to reduce parasite burden) and remain susceptible to clinical malaria in a homologous re-challenge model.

Re-challenge triggers a hardwired emergency myeloid response

The absence of anti-parasite immunity means that any change in the host response to re-challenge must occur independently of pathogen load. Our model therefore provides the ideal setting in which to investigate host adaptations that confer disease tolerance. One route to tolerance may be to reduce systemic inflammation - this correlates with clinical immunity in endemic regions (11) but whether it also coincides with immunity to severe disease is not known. In human challenge studies the immune response detected in whole blood at the peak of infection is largely driven by activated monocytes and neutrophils, which are in transit from the bone marrow (site of activation) (21) to the spleen (target organ) (22). To capture this acute phase response we used whole blood RNA-sequencing and DESeq2 to identify differentially expressed genes at diagnosis (relative to baseline) in first, second and third infection. We found a remarkably similar pattern of interferon-stimulated type I inflammation regardless of infection number (figure 2 - supplement 1). Furthermore, functional

gene enrichment analysis showed that the hierarchy of GO terms was near-identical between infections (figure 2A). This emergency myeloid response has been extensively described in naive hosts infected with *P. falciparum* (13, 23, 24) and *P. vivax* (Bach *et al.*, under review, preprint available at doi.org/10.1101/2021.03.22.21252810) but it was surprising to see no obvious change upon re-challenge. Nevertheless, by analysing each infection independently it was possible that we were missing important quantitative differences and we therefore performed direct pairwise comparisons between first, second and third infection. Initially, we compared each pre-infection time-point to identify season-dependent shifts in baseline gene expression - we found zero differentially expressed genes between infections (adj $p < 0.05$ and absolute fold change > 1.5). When we then compared each diagnosis time-point to identify adaptations in the host response we again found zero differentially expressed genes (figure 2B); evidently, the first three infections of life trigger a hardwired emergency response that is not influenced by season or previous exposure.

Nonetheless, host control of inflammation may not be transcriptionally regulated and we therefore directly measured systemic inflammation at protein level using a highly multiplexed custom bead array (39 plasma analytes indicative of inflammation, coagulation, oxidative stress & metabolism). By analysing the concentration of each analyte through time we found many of the prototypical products of monocyte and neutrophil activation (such as CXCL10, IL-1RA & MPO) were significantly increased at diagnosis, together with hallmark cytokines associated with innate lymphoid cell (ILC) or T cell activation (IFNɣ and IL-21) (figure 2C and figure 2 - supplement 2). Surprisingly, our data seemed to suggest that this response was not attenuated but enhanced upon re-challenge. To directly test this hypothesis we fitted a linear mixed-effects model for each analyte, which showed that the major secreted products of interferon-stimulated inflammation were significantly increased in second and third (compared to first) infection (figure 2D). Collectively, these data demonstrate that *P. falciparum* triggers a hardwired emergency myeloid response throughout the first three infections of life. And crucially, we find no evidence that systemic inflammation can be attenuated to quickly establish disease tolerance.

Malaria uncouples T cell activation from systemic inflammation

Our data do not exclude the importance of minimising systemic inflammation to improve clinical outcome but indicate that long-term exposure to parasites is required to restrict an inflammatory myeloid response (12). These data may partially explain why immunity to clinical malaria is not usually established until adolescence. So what other host adaptations could be acquired early in life to promote immunity to severe disease? To answer this question we examined adaptive T cells, which are inherently plastic, proliferative and long-lived, and therefore uniquely placed to quickly and permanently alter the host response to infection. The acute phase response to malaria causes extreme lymphopenia leading to a 30 - 70% loss of circulating T cells at the peak of infection (figure 1 - supplement 1). The majority of these cells are recruited to the inflamed spleen (25) and it is therefore difficult to assess T cell activation and differentiation at diagnosis. Instead, we need to analyse T cell activation after drug treatment when the myeloid response begins to resolve and T cells return to the circulation. At this time-point, analysing T cell phenotypes in whole blood can provide a direct readout of tissue-specific immune responses in human malaria.

148 Post-treatment blood samples were not available from this cohort of volunteers in their first infection
149 but were collected 6-days after drug treatment of either their second or third malaria episode. We
150 therefore had to recruit new malaria-naive controls to provide time-matched post-treatment samples
151 of first infection and switched to a cross-sectional study design with 11 volunteers infected
152 contemporaneously (3 first infection, 2 second infection and 6 third infection during the VAC063C
153 trial) (see methods and supplementary file 1). Six days after drug treatment (designated T6)
154 lymphopenia had completely resolved and there was no evidence of delayed onset anaemia (figure
155 3A and figure 3 - supplement 1A). All other clinical symptoms of malaria (inc. fever) also resolved
156 and markers of systemic inflammation had returned almost entirely to baseline - this was observed
157 in every volunteer regardless of infection number (figure 3 - supplement 1B). It was therefore a
158 surprise to find a large transcriptional signature in whole blood at T6, which was equal in size to the
159 emergency myeloid response captured at diagnosis (figure 3 - supplement 2A). These signatures
160 did not overlap and instead the differentially expressed genes at T6 had unique functional enrichment
161 terms relating to cell cycle and nuclear division (figure 3 - supplement 2B-C). Remarkably, this
162 proliferative burst was only observed in volunteers undergoing their first infection of life (figure 3 -
163 supplement 3).

164 Myeloid cells are generally terminally differentiated and do not proliferate after their release from the
165 bone marrow; it therefore seemed likely that our whole blood RNA-sequencing data were capturing
166 the return of activated T cells to the circulation. To explore this further we sorted $CD4^+$ T cells with a
167 naive ($CCR7^{pos}$ $CD45RA^{pos}$), effector / effector memory (EM) ($CCR7^{neg}$ $CD45RA^{neg}$) or regulatory
168 ($CD25^{hi}$ $CD127^{neg}$) phenotype one day before challenge and six days post-treatment. Analysis of the
169 cell surface markers used for sorting revealed dramatic activation of effector / EM and regulatory
170 subsets in first infection but not reinfection (figure 3B and figure 3 - supplement 4). These data
171 suggested that T cell activation and systemic inflammation could be uncoupled in malaria. To directly
172 test this hypothesis we constructed a pearson correlation matrix and included all plasma analytes
173 that were significantly up- or downregulated at diagnosis or T6 together with the frequency of
174 activated effector and regulatory $CD4^+$ T cells (figure 3C). Also included were hallmark symptoms of
175 clinical malaria such as pyrexia, lymphopenia and anaemia. We found a strong and significant
176 positive correlation between markers of myeloid cell activation (inc. CXCL10, IL-1RA & TNFRII),
177 coagulation (D-Dimer) and maximum core temperature ($r > 0.7$ and $p < 0.05$). Moreover, each of
178 these features negatively correlated with lymphocyte counts and haemoglobin. In contrast, activated
179 effector and regulatory $CD4^+$ T cells did not correlate with any feature of the acute phase response
180 (supplementary file 2). The intensity of inflammation therefore scales with clinical symptoms but does
181 not influence $CD4^+$ T cell activation.

182 **T_H1 polarisation is a unique feature of first infection**

183 Naive adults are highly susceptible to severe malaria (15) and our data clearly show that the unique
184 feature of their response to infection is fulminant T cell activation. To explore the transcriptional
185 landscape of activated $CD4^+$ T cells in first infection (compared to third) we undertook RNA-
186 sequencing on the naive, effector / EM and regulatory subsets that we had sorted during the
187 VAC063C trial (figure 3 - supplement 4) and used DESeq2 to identify differentially expressed genes
188 at T6 (versus baseline). As expected, cells with a naive phenotype displayed few transcriptional
189 changes upon their return to circulation; in contrast, we found almost 6000 differentially expressed
190 genes in effector / EM $CD4^+$ T cells (adj $p < 0.05$ and > 1.5-fold change). Functional gene enrichment

191 analysis showed that effector cells were proliferative, metabolically reprogrammed and highly
192 activated in first infection, upregulating each of the major costimulatory and inhibitory receptors
193 required to control their fate (figure 4A and figure 4 - supplement 1). Moreover, they specifically
194 upregulated the signature chemokine receptors and transcription factors associated with T_H1
195 polarisation (figure 4B). The cytokines IFNɣ and IL-21 were also both strongly induced, which could
196 indicate that infection stimulates double-producers (26) or that activated follicular helper T cells are
197 also released from the spleen (figure 4C).

198 In third infection IFNɣ and IL-21 were once again significantly upregulated at T6 together with TNF
199 and T_H1-associated chemokine receptors (figure 4B-C). $CD4^+$ T cells are thus clearly responsive to
200 re-challenge despite the lack of evidence for their activation by flow cytometry (figure 3B). Yet
201 remarkably, the transcription factors that drive T_H1 differentiation (T-bet and STAT1) were no longer
202 induced, and neither were the costimulatory molecules or inhibitory receptors observed in first
203 infection (figure 4A-B). So what modifies $CD4^+$ T cell activation to avert T_H1 polarisation upon re-
204 challenge? We found no transcriptional evidence that T cells are quiescent or anergic in third
205 infection and crucially the transcription factors that epigenetically enforce exhaustion were not
206 upregulated (figure 4A and figure 4 - supplement 2A-B). Furthermore, there was no evidence for
207 activation induced cell death - this feature was unique to first infection (figure 4 - supplement 2C).
208 There was also no evidence that effector $CD4^+$ T cells were diverted towards a regulatory fate; for
209 example, hallmarks of T_R1 differentiation (such as Eomes and IL-10) were absent (figure 4B-C).

210 An alternative explanation could be suppression by conventional regulatory $CD4^+$ T cells yet our
211 data show that Tregs simply mirror the response of effector cells. Their activation is tightly co-
212 regulated (figure 3C) and in first infection Tregs launch a transcriptional programme with remarkable
213 overlap to that of effectors (e.g. they upregulate all signature T_H1 genes including T-bet) (figure 4D).
214 In contrast, we could find no transcriptional evidence of Treg activation upon re-challenge. It is well
215 established that regulatory T cells mimic the transcriptional response of the effector cells they are
216 required to regulate (27) and this phenomenon is clearly evident in naive hosts. In fact, by
217 constructing a merged gene ontology network that uses all of the differentially expressed genes
218 identified in effector/EM and regulatory $CD4^+$ T cells we could show that Tregs do not display any
219 unique functional terms (figure 4E). We therefore conclude that regulatory T cells are redundant
220 during reinfection and that their activation is not required because there is no explosive effector
221 response to keep in check. Instead, it would seem that tolerised hosts launch a specialised adaptive
222 T cell programme that can maintain cytokine production without causing extensive activation,
223 proliferation or T_H1 polarisation. Remarkably, we can identify this major shift in the host response in
224 whole blood (figure 4F) and it will therefore be possible to identify tolerised hosts in an endemic
225 setting without the need for complex cell isolation protocols.

226 **Tolerance minimises effector T cell heterogeneity**

227 One limitation of bulk RNA-sequencing is that it can not reveal the heterogeneity of an immune
228 response; this is particularly problematic for $CD4^+$ T cells, which are inherently diverse and plastic.
229 Furthermore, there is very little power to detect transcriptional changes if only a small proportion of
230 cells are activated, as seemed to be the case in third infection. We therefore used mass cytometry
231 to undertake single cell analysis of T cell activation through first and third infection. Importantly, we

designed an antibody panel that would allow us to interrogate every T cell lineage, and examine the key markers of activation, differentiation and fate (supplementary file 3). We first concatenated all data (from every volunteer and time-point) and used Uniform Manifold Approximation and Projection (UMAP) to visualise the phenotypic diversity of T cells across the dataset. We then used FlowSOM clustering to assign each T cell to one of 49 discrete clusters (figure 5 - supplement 1). As expected most of the diversity was observed within the non-naive $CD4^+$ and $CD8^+$ T cell subsets (figure 5A). Tracking the frequency of each cluster through time then resolved dynamic changes in the T cell compartment (figure 5 - supplement 2 for $CD4^+$ T cells, supplement 3 for $CD8^+$ T cells and supplement 4 for innate-like T cells). Finally, we performed linear regression on cell count data using EdgeR to identify the differentially abundant clusters at each time-point relative to baseline (FDR < 0.05 and absolute fold-change > 2).

In first infection eighteen T cell clusters increased in abundance at T6 and all had an activated phenotype; these were comprised of twelve adaptive and six innate-like clusters. In third infection, twelve clusters increased in abundance and not one was unique to re-challenge (all were significant in first infection). Remarkably, we found that diversity was specifically reduced in the adaptive T cell response with only six adaptive clusters called as significant in third infection. Moreover, of these six clusters all but one was reduced in size compared to first infection (figure 5B-C). This means that activated $CD4^+$ T cells dominate the response of naive hosts to malaria whereas in tolerised hosts the T cell response largely consists of innate-like cells (figure 5D). So how do the phenotypes of activated $CD4^+$ T cells compare between infections? We observed enormous heterogeneity in first infection with the expansion of nine distinct $CD4^+$ T cell clusters. There were common traits (such as expression of the activation marker CD38 and the memory marker CD45RO) and most had an effector ($CCR7^{neg}$) phenotype but many clusters displayed unusual or unexpected features (figure 5E). As one example, the largest pool of activated $CD4^+$ T cells had a highly differentiated $CD27^{neg}$ $CX3CR1^{pos}$ cytotoxic phenotype, which is usually observed in autoinflammatory conditions (not infectious disease) (28, 29). Notably, the upregulation of perforin and granzyme B could be seen in $CD4^+$ T cells by RNA-sequencing (figure 4C) and there were many other areas of concordance between the datasets. Most importantly, our protein data confirmed that effector $CD4^+$ T cells were highly activated ($CD28^{hi}$ $PD1^{hi}$), T_H1 polarised (T-bet^{hi}), proliferative ($Ki67^{hi}$) and accompanied by the activation of $Foxp3^{hi}$ $CD39^{hi}$ T-bet^+ regulatory T cells.

In contrast, the unusual $CD4^+$ T cell phenotypes observed in naive hosts were essentially absent in third infection and there was no expansion of activated Tregs (figure 5C). Instead, the majority of expanded $CD4^+$ T cells belonged to a single cluster with an apparently benign effector phenotype ($ICOS^{neg}$ $Ki67^{neg}$ T-bet^{lo} $Eomes^{neg}$) (figure 5E). These cells are clearly activated ($CD38^{hi}$ $Bcl2^{lo}$) and had already increased in abundance at diagnosis (figure 5 - supplement 2). A faster response may indicate that these are malaria-specific memory cells. Furthermore, as the dominant activated cluster these $CD4^+$ T cells are likely to be responsible for most of the transcriptional changes in the effector / EM subset in third infection, including cytokine production (figure 5D and figure 4C). To validate these phenotypic observations we used *limma* to model differential marker expression through time (figure 5 - supplement 5). This analysis confirmed widespread upregulation of activation and differentiation markers in effector / effector memory and regulatory T cells in first infection but an attenuated response to re-challenge (figure 5 - supplement 5 and 6).

Collectively, these data show that tolerance leads to a smaller and less diverse adaptive T cell response. Although at first glance this may seem counterintuitive we argue that this is a more proportional host response designed to support the development of humoral immunity (long-term goal) whilst providing short-term protection against collateral damage. After all, it is essential to prioritise host fitness when infected with a pathogen that can not be cleared and the functionally diverse $CD4^+$ T cell response triggered in naive hosts does not appear to be beneficial (there is no evidence for reduced pathogen load or improved clinical outcome during a first-in-life infection in this study or endemic settings (30)). Moreover, the frequency of $CD38^{hi}$ $CD4^+$ T cells in third infection is not small (it is comparable to typhoid fever (31)) and effector cells have retained critical helper functions (IFNɣ and IL-21). It therefore appears that the adaptive response of a naive host is atypical leading to the activation of 20 - 40% of every T cell in circulation (figure 5F) and the generation of cytotoxic effectors previously associated with immune-mediated disease.

Controlling T cell activation protects host tissues

To directly test whether T cell activation in first infection could be pathological we measured biomarkers of collateral tissue damage, a common histological feature of severe malaria. The blood-stage of infection frequently causes liver injury in naive hosts (32-34) and auto-aggressive human T cells can directly kill hepatocytes through TCR-independent mechanisms (35) - we therefore measured alanine aminotransferase (ALT) to provide a readout of hepatocellular death in our cohort. In first infection, two out of three volunteers had abnormal ALT (more than the upper limit of the reference range) when activated T cells were released from inflamed tissues at T6 (figure 6A). This was accompanied by increased gamma-glutamyl transferase (GGT) and aspartate aminotransferase (AST) leading to moderate or severe adverse events in both volunteers. In contrast, there was little evidence of any deviation from baseline in liver function tests after re-challenge. A meaningful statistical comparison between naive and tolerised hosts was not possible due to the small sample size in first infection (n = 3) and we therefore performed a meta-analysis using a previously published surrogate dataset (33). Specifically, we examined post-treatment ALT measurements in almost 100 volunteers experiencing a first-in-life infection as part of a human challenge study. Importantly, we only included CHMI trials that were directly comparable to our own re-challenge study - that is to say that the same clonal parasite genotype was used (3D7 or the parental NF54 line); parasites had recently been transmitted through the vector; and the same study end-points were applied (treatment at around 10,000 parasites ml^{-1}) (figure 6B). Remarkably, we found that the prevalence of abnormal ALT was reduced from 75% during first infection to 25% upon re-challenge (figure 6C). And in those rare cases where ALT was increased in second or third infection adverse events were mild (not moderate or severe) even though pathogen load was increased (figure 6B). These data thus show that the risk of tissue damage and injury can be significantly reduced in the absence of parasite control. Here then is *in vivo* evidence that long-lived mechanisms of disease tolerance operate in human malaria and can be acquired after a single infection. Moreover, protection does not require the attenuation of systemic inflammation but instead coincides with host control of T cell activation.

Discussion

It has long been recognised that immunity to severe malaria is acquired early in life, offers protection against all manifestations of severe disease and usually precedes clinical immunity (the transition to asymptomatic infection) by more than a decade (2-5). We also know that immunity to severe malaria does not require improved parasite control (1) and is thus underpinned by acquired mechanisms of disease tolerance. This is an important distinction to make if we want to understand how to reduce malaria mortality. Host control of inflammation could provide a rapid route to disease tolerance but our data show that malaria parasites trigger a hardwired emergency myeloid response across the first three infections of life. In contrast, $CD4^+$ T cell activation is quickly modified to limit the number and diversity of effector cells. Our pilot data from a re-challenge model using *P. vivax* shows the same attenuation of $CD4^+$ T cells after a single infection (figure 6 - supplement 1). Exposure-dependent control of T cell activation therefore occurs independently of parasite species, pathogen load and systemic inflammation. Importantly, tolerance does not silence the adaptive response to re-challenge (cytokine-producing T-bet^{lo} EM $CD4^+$ T cells are re-activated) but avoids cell fates associated with collateral damage and autoinflammatory disease. Whilst we can't directly show that this reduces the risk of severe malaria in a human challenge model the epidemiology of *P. falciparum* clearly shows that disease tolerance can be established within the first three infections of life (1, 36).

So how is the adaptive T cell response to malaria modified so quickly and so dramatically? One possibility is that infection initiates heritable epigenetic programmes that reduce T cell responsiveness. Our data do not provide transcriptional evidence of anergy or exhaustion but this hypothesis needs to be directly tested. An alternative explanation could be the clonal deletion of activated T cells during first infection reducing the number of malaria-specific clones available for re-challenge. Or perhaps, tolerance requires no T cell-intrinsic modifications but an attenuation of the antigen presenting capacity of the spleen. After all, hemozoin-loaded dendritic cells and macrophages have a reduced capacity to stimulate T cell proliferation *in vitro* (37). Long-term modifications to the tissue environment (12) (including the presence of malaria-specific antibodies) may also impact T cell differentation and block the development of terminally differentiated pathogenic effectors. Nonetheless, the activation of T-bet^{lo} EM $CD4^+$ T cells (and production of IFNɣ and IL-21) may be sufficient to support the gradual acquisition of humoral immunity in tolerised hosts. Perhaps then we are asking the wrong question and should instead examine how malaria can drive such extensive and diverse T cell activation in a naive host.

One possibility is that infection leads to widespread bystander activation of $CD4^+$ T cells that do not recognise malaria antigens. These could be pre-existing memory cells, which can be activated in the absence of TCR signals and costimulation (38, 39). This would certainly explain the speed, magnitude and heterogeneity of T cell activation in our naive volunteers. And furthermore, it may explain the increased susceptibility of adults to severe disease during a first-in-life infection (they have a far larger memory pool than infants and children). Malaria may also cause activation of autoreactive T cells, which would need to be quickly suppressed by activated Tregs in first infection. Central tolerance (which deletes autoreactive clones in the thymus) is only partially effective and there is enormous degeneracy in TCR reactivity (40). Systemic infection with a pathogen carrying more than 5000 protein-coding genes may therefore lead to considerable cross-reactivity between parasite and host. Indeed, hypergammaglobulinemia and autoantibody production are known

features of human malaria (41, 42). We therefore propose that bystander and cross-reactive T cells may account for the majority of T cell activation in naive hosts. And because they can be activated via TCR-independent or low affinity interactions (39, 43) it might be possible to specifically silence their pathogenic response without impeding re-activation of high affinity malaria-specific clones. Support for this idea comes from the observation that *P. chabaudi* triggers massive polyclonal activation of $CD4^+$ T cells in first infection but not reinfection in mice (44).

Importantly, we have shown that parasite species regulates T cell activation in naive hosts - *P. falciparum* drives a bigger $CD4^+$ T cell response with more functional diversity than *P. vivax* even though they trigger a near-identical myeloid response (Bach *et al*., under review, preprint available at doi.org/10.1101/2021.03.22.21252810). A combination of increased sequestration and T cell activation could therefore underpin the increased virulence of *P. falciparum*. This could explain why large multi-centre genome-wide association studies have failed to identify SNPs in immune genes that can predict susceptibility to severe malaria (45). Variation in human T cells is almost exclusively driven by non-heritable factors (46). And it may also explain how immunity to severe malaria can be acquired so quickly. Exposure-dependent control of T cell activation could reduce tissue damage, endothelium activation and toxicity to minimise the harm caused by cytoadherence. Crucially, our data show that a single asymptomatic drug-cured infection is sufficient to silence pathogenic T cells. Interventions that reduce the risk of clinical malaria but don't completely eliminate infection (such as mass drug administration) may thus induce long-lived mechanisms of disease tolerance in endemic settings.

Acknowledgements

We thank Paul Sopp for *ex vivo* T cell sorting during the VAC063 trial. Flow sorting and CyTOF data were generated within the flow and mass cytometry facilities at the Weatherall Institute of Molecular Medicine (University of Oxford), which are supported by MRC Human Immunology Unit core funding (MC_UU_00008) and the Oxford Single Cell Biology Consortium (OSCBC). T cell RNAseq libraries were prepared and sequenced by the Edinburgh Clinical Research Facility at the University of Edinburgh, which receives financial support from NHS Research Scotland (NRS). Whole blood RNAseq libraries were prepared and sequenced by Edinburgh Genomics, which is supported through core grants from NERC (R8/H10/56), MRC UK (MR/K001744/1) and BBSRC (BB/J004243/1). We would like to extend our thanks to the VAC063 and VAC069 clinical and laboratory teams for assistance, and to all of the volunteers who participated in this study.

Funding

The VAC063 and VAC063C trials were supported in part by the Office of Infectious Diseases, Bureau for Global Health, U.S. Agency for International Development (USAID) under the terms of the Malaria Vaccine Development Program (MVDP) contract AID-OAA-C-15-00071, for which Leidos, Inc. is the prime contractor. The opinions expressed herein are those of the authors and do not necessarily reflect the views of the USAID. The clinical trial was also supported in part by the National Institute for Health Research (NIHR) Oxford Biomedical Research Centre (BRC). The views expressed are those of the authors and not necessarily those of the NIHR or the Department of Health and Social Care. The VAC069 trial was supported by funding from the European Union's Horizon 2020 research and innovation programme under grant agreement for MultiViVax (number 733073). DMS is the recipient of a Darwin Trust of Edinburgh PhD studentship. FB is the recipient of a Wellcome Trust PhD studentship (grant no. 203764/Z/16/Z). SJD held a Wellcome Trust Senior Fellowship (grant no. 106917/Z/15/Z) and is a Jenner Investigator. And PJS is the recipient of a Sir Henry Dale Fellowship jointly funded by the Wellcome Trust and the Royal Society (grant no. 107668/Z/15/Z).

Data availability

All RNAseq data (whole blood and sorted T cell subsets) have been deposited in NCBI's Gene Expression Omnibus and are accessible through GEO SuperSeries accession number GSE172481. CyTOF (mass cytometry) data have been deposited at flowrepository.org and can be accessed through experiment numbers FR-FCM-Z47Z (VAC063C); FR-FCM-Z3HA (VAC069A); and FR-FCM-Z465 (VAC069B).

The authors have no conflict of interest to declare and the funders had no role in study design, data interpretation or the decision to submit the work for publication.

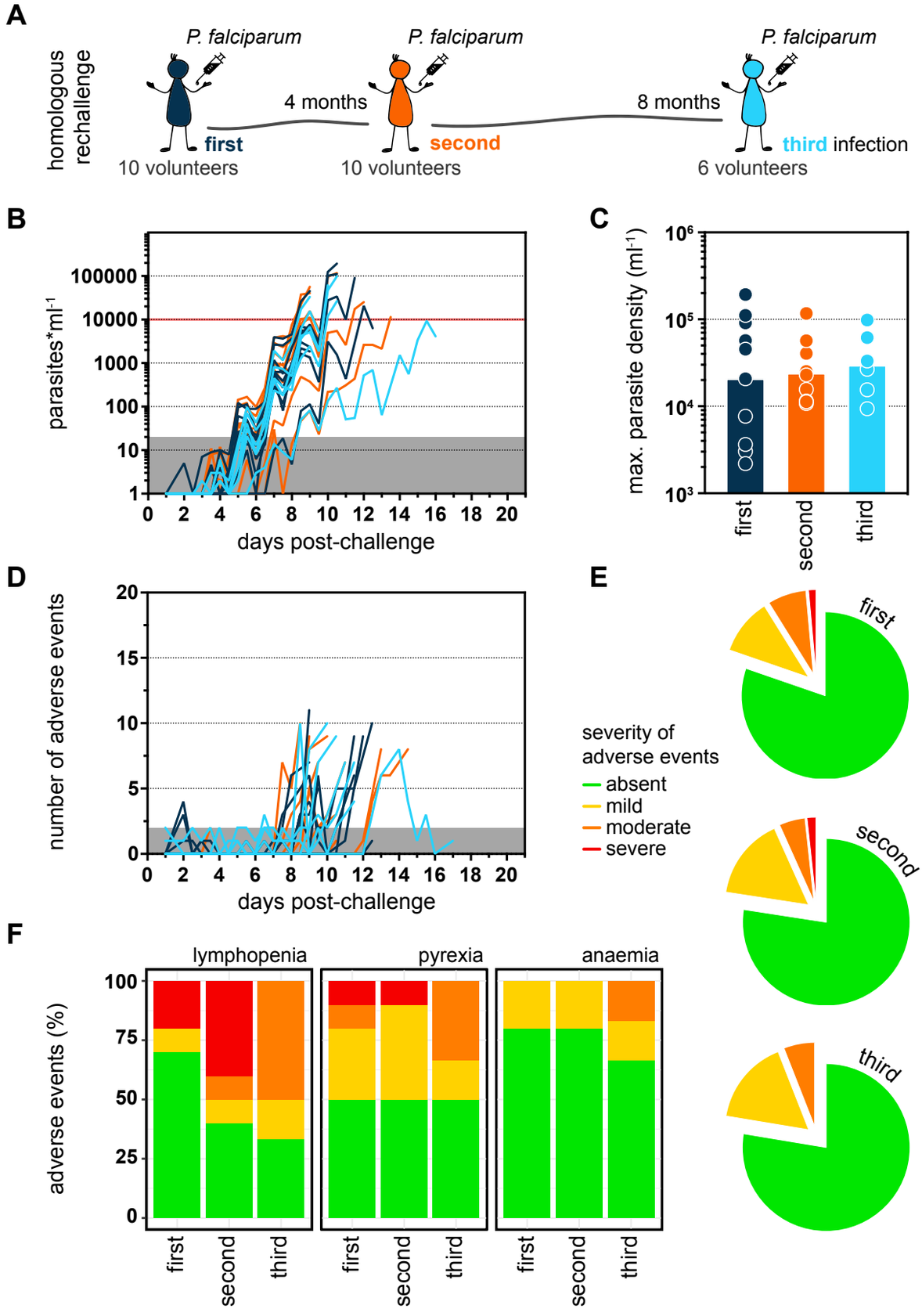
A
homologous rechallenge
P. falciparum
P. falciparum
P. falciparum
4 months
8 months
first
second
third infection
10 volunteers
10 volunteers
6 volunteers
B
parasites*ml-1
days post-challenge
C
max. parasite density (ml-1)
first
second
third
D
number of adverse events
days post-challenge
E
severity of adverse events
absent
mild
moderate
severe
first
second
third
F
adverse events (%)
lymphopenia
pyrexia
anaemia
first
second
third

figure one

Figure 1 | Malaria does not induce fast-acting mechanisms of host resistance. (**A**) Healthy malaria-naive adults were infected up to three times with *P. falciparum* (clone 3D7) by direct blood challenge. Repeated sampling before, during and after each infection allowed us to track the development of disease tolerance in real-time. (**B**) Parasite growth curves for first, second and third infection (each line represents a volunteer and lines are colour-coded by infection number). Parasite density in whole blood was measured by qPCR every 12-hours - the grey box represents the lower limit of quantification (20 parasites*ml^{-1}) and the treatment threshold of 10,000 parasites*ml^{-1} is denoted by the pink line. (**C**) Maximum parasite density during first, second and third infection; each dot represents a volunteer and bars show the median. No statistically significant difference between infections was observed (Kruskal-Wallis test $p = 0.9054$). (**D**-**F**) Clinical symptoms of malaria were recorded on diary cards (self-reporting) or during clinic visits; these adverse events were graded as mild, moderate, or severe (see methods). (D) Number of adverse events at each time-point throughout infection and up to 48-hours after treatment (each line represents a volunteer and lines are colour-coded by infection number). (E) Severity of adverse events in the 48-hours before and after diagnosis in first, second and third infection. (F) Frequency and severity of lymphopenia, pyrexia and anaemia during first, second and third infection. No statistically significant difference between infections was observed for any adverse event (Kruskal-Wallis test using a significance threshold of 5%). In (B-F) sample size (n) is 10 (for first and second infection) and 6 (third infection).

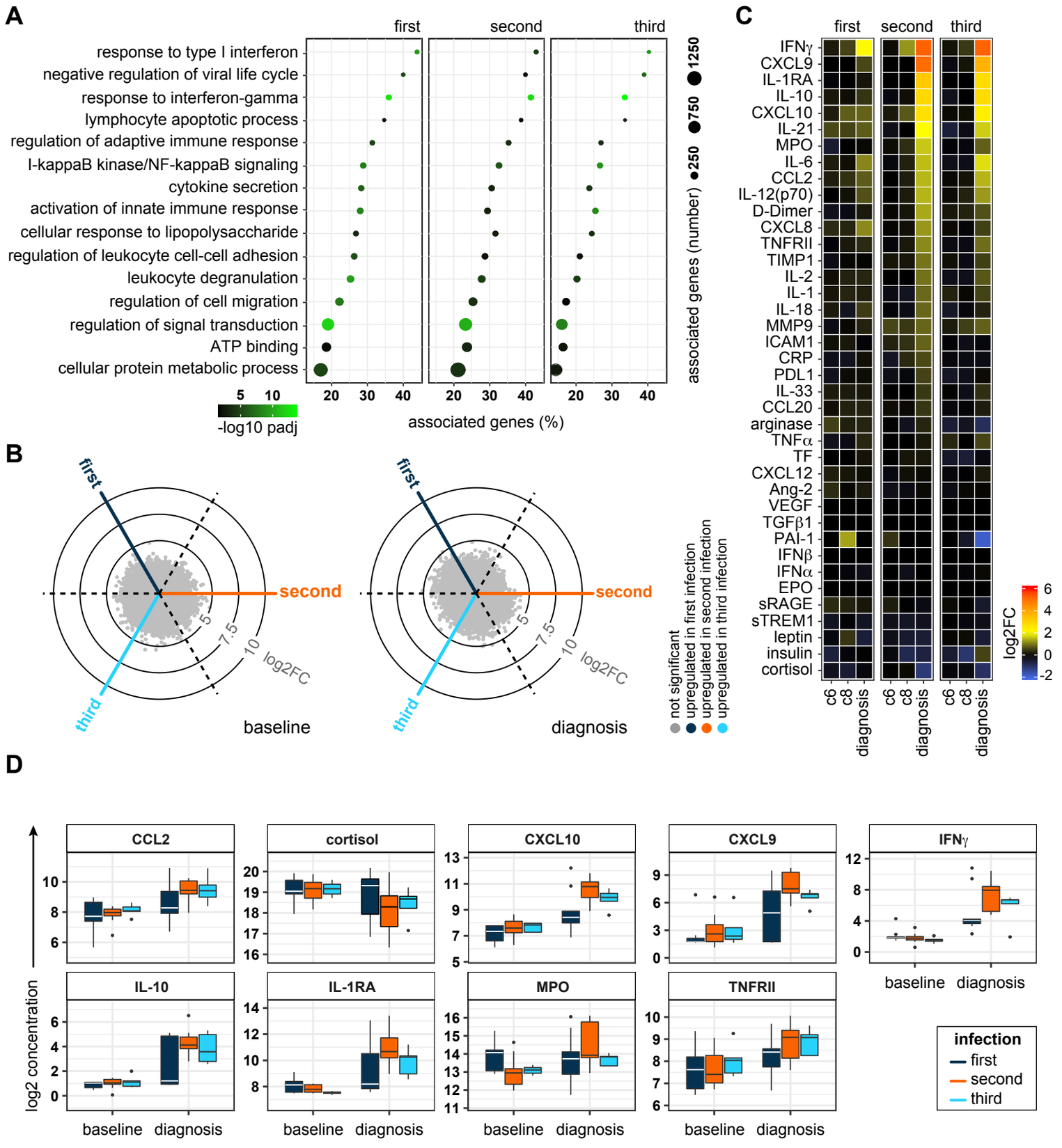
A
first
second
third
response to type I interferon
negative regulation of viral life cycle
response to interferon-gamma
lymphocyte apoptotic process
regulation of adaptive immune response
I-kappaB kinase/NF-kappaB signaling
cytokine secretion
activation of innate immune response
cellular response to lipopolysaccharide
regulation of leukocyte cell-cell adhesion
leukocyte degranulation
regulation of cell migration
regulation of signal transduction
ATP binding
cellular protein metabolic process
associated genes (number)
1250
750
250
-log10 padj
associated genes (%)
B
first
second
third
log2FC
baseline
diagnosis
not significant
upregulated in first infection
upregulated in second infection
upregulated in third infection
C
IFNγ
CXCL9
IL-1RA
IL-10
CXCL10
IL-21
MPO
IL-6
CCL2
IL-12(p70)
D-Dimer
CXCL8
TNFRII
TIMP1
IL-2
IL-1
IL-18
MMP9
ICAM1
CRP
PDL1
IL-33
CCL20
arginase
TNFα
TF
CXCL12
Ang-2
VEGF
TGFβ1
PAI-1
IFNβ
IFNα
EPO
sRAGE
sTREM1
leptin
insulin
cortisol
c6
c8
diagnosis
log2FC
D
CCL2
cortisol
CXCL10
CXCL9
IFNγ
IL-10
IL-1RA
MPO
TNFRII
log2 concentration
baseline
diagnosis
infection
first
second
third

figure two

Figure 2 | Re-challenge triggers a hardwired emergency myeloid response. (**A**) RNA-sequencing was used to identify differentially expressed genes in whole blood at diagnosis versus baseline (adj $p < 0.05$ and > 1.5 fold-change). ClueGO was then used for functional gene enrichment analysis and placed significant GO terms into functional groups by relatedness (see methods). Shown are the leading GO terms from 15 non-redundant groups with the lowest adj p value in first infection. We plotted the same GO terms in second and third infection. Note that each infection was analysed independently. (**B**) Radar plots (or 3-way volcano plots) show the number of differentially expressed genes in whole blood between infections. Direct pairwise comparisons between second and first, third and first and third and second infection were performed - the left plot compares all baseline samples and the right plot the diagnosis time-points. Dashed lines represent the centre-point for each volcano plot and the position of each dot relative to this line shows up- or downregulation. There were no differentially expressed genes in any of the six pairwise comparisons (adj $p < 0.05$ and > 1.5 fold-change). (**C**) 39 plasma analytes were quantified before and during each infection using a highly multiplexed bead-based array. The log2 fold-change of each analyte is shown relative to baseline on day 6 and 8 post-challenge (c6 and c8, respectively) and at diagnosis. Analytes are ordered by log2 fold-change in second infection. (**D**) Mixed-effects modelling was used to identify plasma analytes that vary significantly between infections at diagnosis. Multiple test correction was performed using the Benjamini-Hochberg method and analytes that were significant in both second and third infection (versus first infection) are shown (adj $p < 0.05$). Box (median and IQR) and whisker (1.5x upper or lower IQR) plots are shown with outliers as dots. In (A-B) n = 10 (first infection), 9 (second infection) and 6 (third infection). v1040 was excluded from RNA-sequencing analysis in second infection because their baseline sample failed QC. In (C-D) n = 9 (first and second infection) and 5 (third infection). v1040 was excluded from plasma analysis because all samples failed QC (see methods).

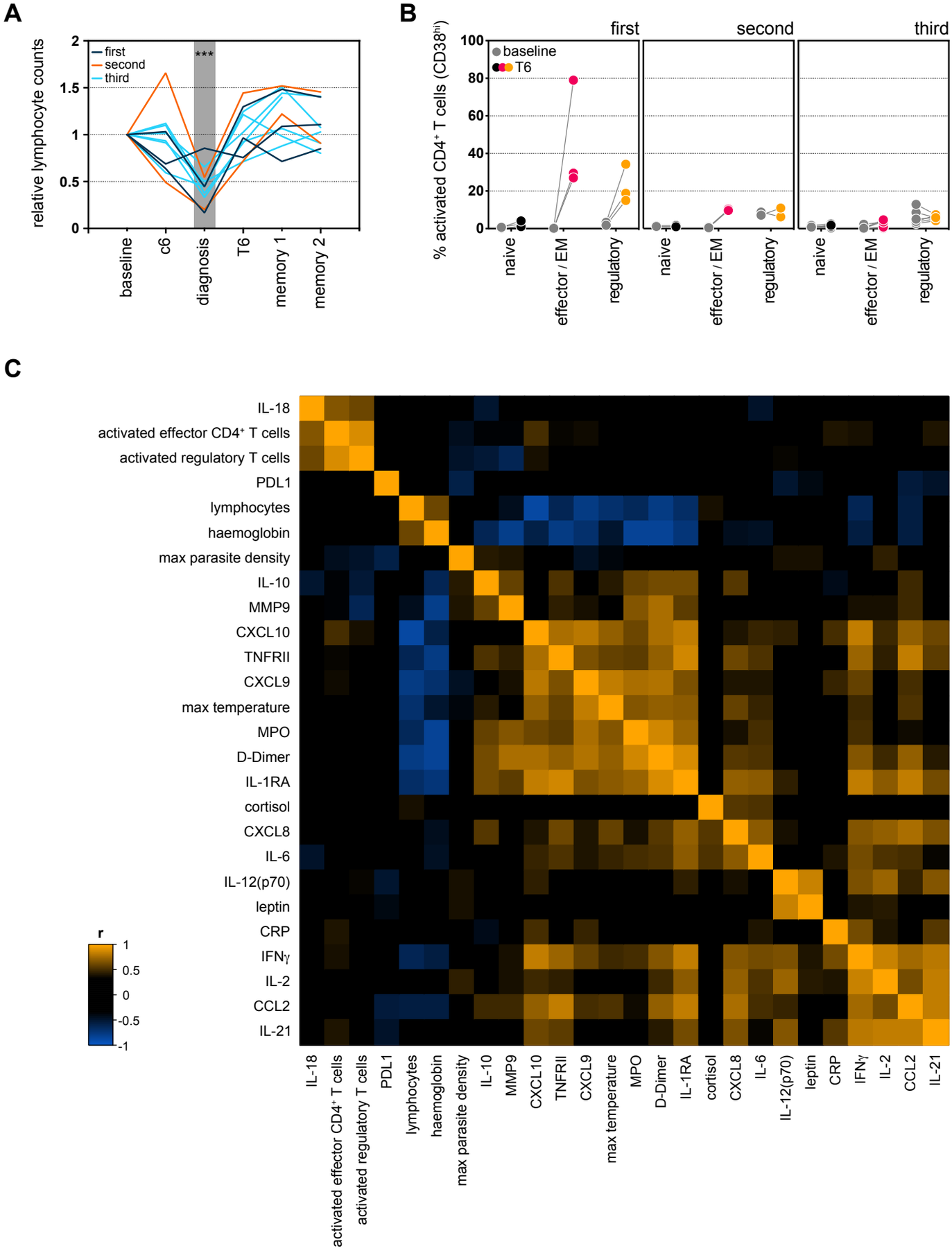

figure three

Figure 3 | Malaria uncouples T cell activation from systemic inflammation. (**A**) Lymphocytes were quantified in whole blood 6-days post-challenge (c6), at diagnosis, 6-days after treatment (T6) and at two memory time-points (45 and 90-days post-challenge). Counts were normalised to baseline measurements (taken one day before challenge). Each line represents a volunteer and lines are colour-coded by infection number. A statistically significant deviation from baseline was observed only at diagnosis (Wilcoxon matched-pairs signed rank test, *** $p < 0.001$). (**B**) The percentage of activated $CD38^{hi}$ $CD4^{+}$ T cells was analysed by flow cytometry at baseline (grey dots) and T6 (coloured dots). Data are shown for naive, effector/effector memory (EM) and regulatory subsets in volunteers undergoing their first, second or third infection of life (see figure 3 - supplement 4 for gating strategies). (**C**) Pearson correlation matrix of the log2 transformed fold-change of lymphocytes, haemoglobin and differentially abundant plasma analytes. Fold-change was calculated either at diagnosis or T6 (relative to baseline) according to when this was largest for each feature. Also included is maximum parasite density, maximum core temperature (up to 48-hours post-treatment) and the percentage of activated effector and regulatory $CD4^{+}$ T cells (at T6). The order of features was determined by hierarchical clustering. In (A-B) n = 11 (3 first infection, 2 second infection and 6 third infection) and in (C) n = 10 (3 first infection, 2 second infection and 5 third infection). v1040 was excluded from plasma analysis because all samples failed QC.

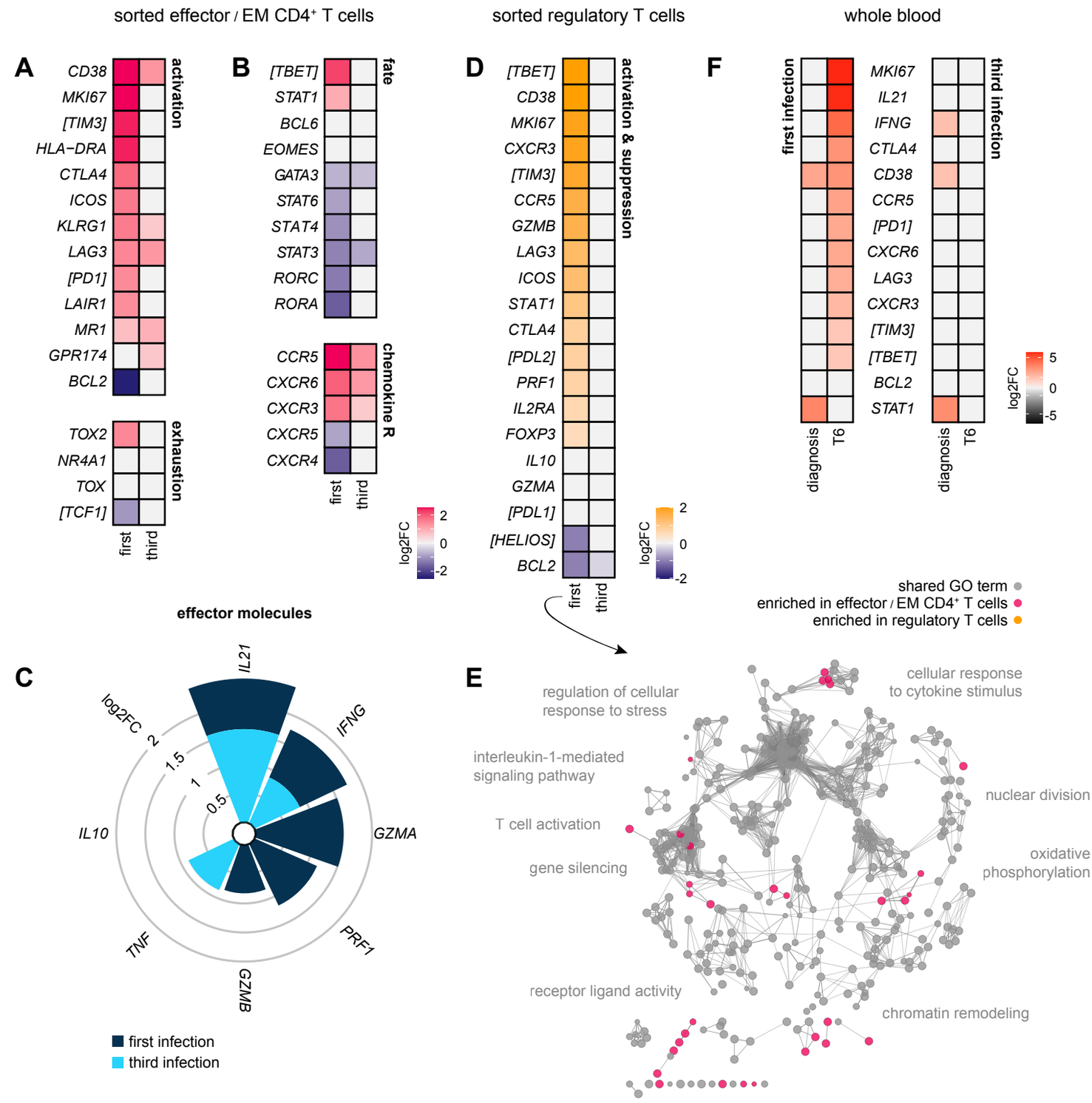
sorted effector / EM CD4+ T cells
sorted regulatory T cells
whole blood
A
CD38
MKI67
[TIM3]
HLA-DRA
CTLA4
ICOS
KLRG1
LAG3
[PD1]
LAIR1
MR1
GPR174
BCL2
activation
TOX2
NR4A1
TOX
[TCF1]
exhaustion
first
third
B
[TBET]
STAT1
BCL6
EOMES
GATA3
STAT6
STAT4
STAT3
RORC
RORA
fate
CCR5
CXCR6
CXCR3
CXCR5
CXCR4
chemokine R
first
third
log2FC
2
0
-2
D
[TBET]
CD38
MKI67
CXCR3
[TIM3]
CCR5
GZMB
LAG3
ICOS
STAT1
CTLA4
[PDL2]
PRF1
IL2RA
FOXP3
IL10
GZMA
[PDL1]
[HELIOS]
BCL2
activation & suppression
first
third
log2FC
2
0
-2
F
first infection
MKI67
IL21
IFNG
CTLA4
CD38
CCR5
[PD1]
CXCR6
LAG3
CXCR3
[TIM3]
[TBET]
BCL2
STAT1
third infection
diagnosis
T6
diagnosis
T6
log2FC
5
0
-5
shared GO term
enriched in effector / EM CD4+ T cells
enriched in regulatory T cells
C
effector molecules
log2FC
2
1.5
1
0.5
IL21
IFNG
GZMA
PRF1
GZMB
TNF
IL10
first infection
third infection
E
regulation of cellular response to stress
cellular response to cytokine stimulus
interleukin-1-mediated signaling pathway
nuclear division
T cell activation
oxidative phosphorylation
gene silencing
receptor ligand activity
chromatin remodeling

figure four

467 **Figure 4** | T_H1 polarisation is a unique feature of first infection. (**A**-**C**) During the VAC063C study
468 RNA-sequencing was used to identify differentially expressed genes in effector / effector memory
469 (EM) $CD4^+$ T cells 6-days after parasite clearance (T6 versus baseline) in first and third infection (adj
470 $p < 0.05$ and > 1.5 fold-change). Heatmaps show the log2 fold-change of (A) markers of T cell
471 activation and exhaustion and (B) the master transcription factors that shape T cell fate (plus
472 associated chemokine receptors). The stacked circular bar chart in (C) shows the log2 fold-change
473 of cytokines and cytotoxic effectors upregulated in first or third infection. Note that *IL10* is not
474 differentially expressed in either infection. (**D**) RNA-sequencing was used to identify differentially
475 expressed genes in regulatory $CD4^+$ T cells at T6 (versus baseline) in first and third infection (adj p
476 < 0.05 and > 1.5 fold-change). Shown are markers of Treg activation and differentiation plus key
477 suppressor molecules. (**E**) Differentially expressed genes in effector / EM and regulatory $CD4^+$ T cells
478 were combined for GO analysis of T6 in first infection. ClueGO was used to construct a merged
479 functional gene ontology network. Each node represents a GO term and nodes are coloured
480 according to whether their associated genes were majoritively (> 60%) derived from effector or
481 regulatory cells. GO terms that were shared between T cell subsets are coloured grey - nine leading
482 GO terms (each from a unique functional group) that were shared are labelled (see methods). (**F**)
483 RNA-sequencing was used to identify differentially expressed genes in whole blood at diagnosis and
484 T6 (relative to baseline) in first and third infection (adj $p < 0.05$ and > 1.5 fold-change). Signature
485 genes of T cell activation, T_H1 differentation and cytokine production are shown. In (A-E) n = 2 or 3
486 for first infection (T6 and baseline, respectively) and 6 for third infection. v313 was excluded at T6
487 because this sample failed QC. In (F) n = 3 for first infection and 6 for third infection. Square brackets
488 indicate that common gene names were used.

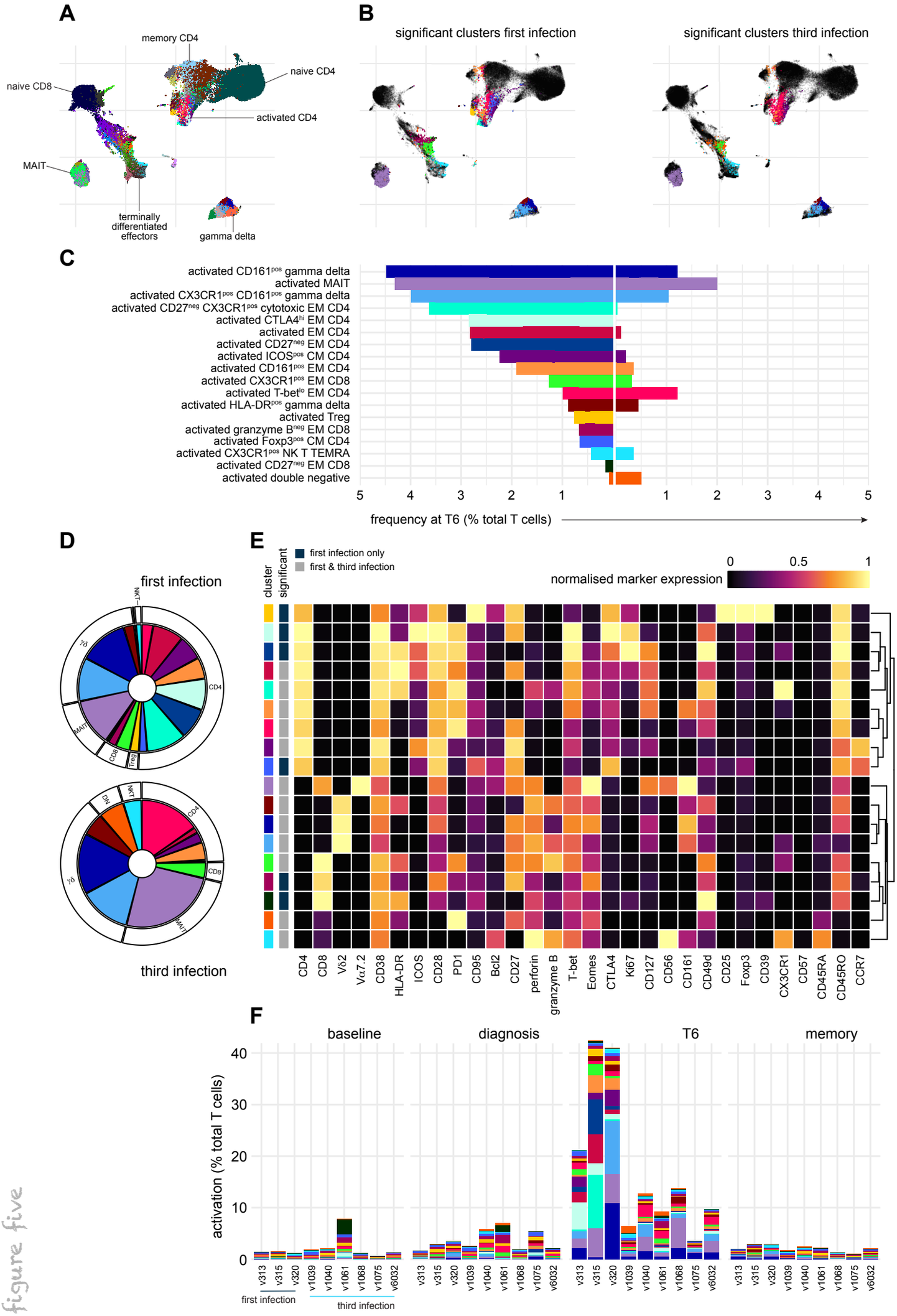
A
memory CD4
naive CD4
naive CD8
activated CD4
MAIT
terminally differentiated effectors
gamma delta
B
significant clusters first infection
significant clusters third infection
C
activated CD161pos gamma delta
activated MAIT
activated CX3CR1pos CD161pos gamma delta
activated CD27neg CX3CR1pos cytotoxic EM CD4
activated CTLA4hi EM CD4
activated EM CD4
activated CD27neg EM CD4
activated ICOSpos CM CD4
activated CD161pos EM CD4
activated CX3CR1pos EM CD8
activated T-betlo EM CD4
activated HLA-DRpos gamma delta
activated Treg
activated granzyme Bneg EM CD8
activated Foxp3pos CM CD4
activated CX3CR1pos NK T TEMRA
activated CD27neg EM CD8
activated double negative
5 4 3 2 1 1 2 3 4 5
frequency at T6 (% total T cells)
D
first infection
NKT
γδ
CD4
MAIT
CD8
Treg
DN
third infection
E
cluster
significant
first infection only
first & third infection
normalised marker expression
0 0.5 1
CD4 CD8 Vδ2 Vα7.2 CD38 HLA-DR ICOS CD28 PD1 CD95 Bcl2 CD27 perforin granzyme B T-bet Eomes CTLA4 Ki67 CD127 CD56 CD161 CD49d CD25 Foxp3 CD39 CX3CR1 CD57 CD45RA CD45RO CCR7
F
baseline
diagnosis
T6
memory
activation (% total T cells)
0 10 20 30 40
v313 v315 v320 v1039 v1040 v1061 v1068 v1075 v6032
first infection
third infection

figure five

Figure 5 | Tolerance minimises effector T cell heterogeneity. Whole blood was preserved within 30-minutes of blood draw at baseline, diagnosis, T6 and 45-days post-challenge (memory time-point) during the VAC063C study. Samples were stained with a T cell focussed antibody panel (see supplementary file 3) and acquired on a Helios mass cytometer. After exclusion of normalisation beads and doublets we gated on $CD45^{pos}$ $CD3^{pos}$ T cells for UMAP projections and FlowSOM clustering. (**A**) Data from all volunteers and time-points was concatenated to generate a UMAP projection showing the global structure of our dataset. FlowSOM identified 49 discrete T cell clusters and each is given a unique colour. The major T cell subsets are labelled according to expression of lineage, memory and activation markers. (**B**) UMAP projection showing the T cell clusters that are differentially abundant at T6 in first (left) and third infection (right) (FDR < 0.05 and > 2 fold-change). Clusters that are not significant are shown in black. (**C**) The mean frequency of each T cell cluster that is differentially abundant at T6 in first and/or third infection is shown as a proportion of all $CD45^{pos}$ $CD3^{pos}$ T cells. (**D**) Pies show the relative size of each differentially abundant cluster at T6 in first (top) and third (bottom) infection. (**E**) Heatmap showing the normalised median expression values of all markers used for clustering in each of the 18 T cell clusters that were differentially abundant at T6. Colour codes to the left of the heatmap indicate cluster identity and show whether clusters were significant in first infection or first and third infection. Note that no cluster was unique to third infection. (**F**) Stacked bar chart showing the frequency of activated ($CD38^{hi}$ $Bcl2^{lo}$) T cell clusters at each time-point. In (A-F) n = 3 for first infection and 6 for third infection.

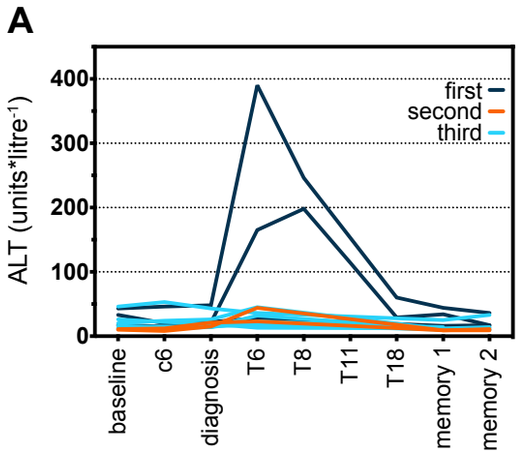

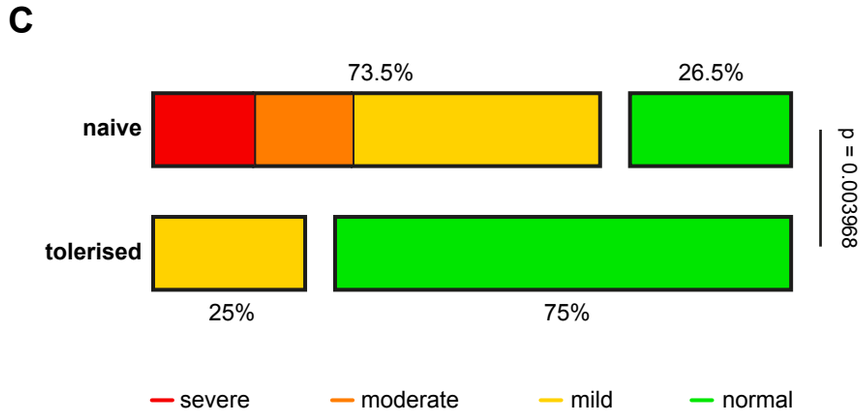

B

	data source	number of volunteers	abnormal ALT [b]	severity			peak parasite density [c]
				mild	moderate	severe	
naive	Reuling *et al.* [a]	95	70	40	16	14	
	VAC063C	3	2	0	0	2	
	Total	**98**	**72**	**40**	**16**	**16**	**17,587**
tolerised	VAC063C	**8**	**2**	**2**	**0**	**0**	**36,630**

[a] studies: EHMI-3, LSA-3, EHMI-8B, EHMI-9, ZonMw2, TIP5 and CHMI-trans1
[b] plasma concentration exceeds the upper limit of the reference range
[c] weighted mean number of parasites per ml whole blood

figure six

508 **Figure 6** | Controlling T cell activation protects host tissues. (**A**) Blood chemistry measured the
509 concentration of alanine aminotransferase (ALT) throughout infection and convalescence in the
510 VAC063C study (baseline, 6-days post challenge (c6), diagnosis, 6 to 18-days after treatment (T6-
511 T18) and 45/90-days post-challenge (memory time-point 1 and 2, respectively)). Each line
512 represents one volunteer and lines are colour-coded by infection number. (**B**) A surrogate dataset
513 from Reuling *et al*. (33) was used to extract information on the frequency and severity of abnormal
514 ALT during a first-in-life infection (up to 6-days post-treatment). All volunteers were infected with *P.*
515 *falciparum* (3D7 or NF54) as part of a CHMI trial that used equivalent end-points to our own study
516 (see methods). In every case, abnormal ALT was scored using the same adaptation of the WHO
517 adverse event grading system. Data from 95 volunteers in Reuling *et al*. and the 3 first infection
518 volunteers in VAC063C were pooled for analysis. (**C**) Frequency and severity of liver injury during
519 first infection (naive hosts) versus re-challenge (tolerised hosts). Barnard's test was used to
520 statistically determine whether an abnormal ALT reading was more prevalent during a first-in-life
521 infection compared to second or third infection (a p value below 0.05 was considered significant). In
522 (A) n = 11 (3 first infection, 2 second infection and 6 third infection) and in (B-C) n = 98 (first infection)
523 and 8 (re-challenge).

524 Methods

525 **Clinical trial design**

526 All volunteers were healthy, malaria naive adults aged between 18 and 50 years and were enrolled
527 in up to three CHMI studies - VAC063A (November 2017), VAC063B (March 2018) and VAC063C
528 (November 2018). The VAC063 protocol encompassed VAC063A and VAC063B, and was an open
529 label, non-randomised phase I/IIa clinical trial evaluating vaccine efficacy of the recombinant blood-
530 stage malaria protein RH5.1 in $AS01_B$ adjuvant (GSK) (47). The VAC063C trial was designed to
531 investigate the durability of any protective anti-parasite immunity measured in control (non-
532 vaccinated) volunteers upon homologous re-challenge (Themistocleous Y *et al*., in preparation). We
533 collected and analysed whole blood samples from 8 control volunteers in VAC063A (all receiving
534 their first infection), 10 control volunteers in VAC063B (8 receiving their second infection and 2 their
535 first infection) and 11 control volunteers in VAC063C (6 receiving their third infection, 2 receiving
536 their second infection and 3 their first infection) (refer to supplementary file 1). The VAC063 and
537 VAC063C trials were sponsored by the University of Oxford. VAC063 received ethical approval from
538 the UK NHS Research Ethics Service (Oxfordshire Research Ethics Committee A, reference
539 16/SC/0345) and was registered on ClinicalTrials.gov (reference NCT02927145). VAC063C
540 received ethical approval from the UK NHS Research Ethics Service (South Central - Oxford A,
541 reference 18/SC/0521) and was also registered on ClinicalTrials.gov (reference NCT03906474). All
542 CHMI studies were conducted in the UK at the Centre for Vaccinology and Tropical Medicine
543 (University of Oxford) and were conducted according to the principles of the current revision of the
544 Declaration of Helsinki 2008 and in full conformity with the ICH Guidelines for Good Clinical Practice.
545 Volunteers signed written consent forms and consent was checked prior to each CHMI. Details of
546 volunteer recruitment, consent, inclusion/exclusion criteria and group allocation can be found in
547 Minassian *et al*. (47).

548 In each CHMI study, all volunteers were infected by direct intravenous inoculation of *P. falciparum*
549 (clone 3D7) blood-stage parasites. The inoculum was thawed and prepared under strict aseptic
550 conditions exactly as described (47, 48) and volunteers received between 452 and 857 infected red
551 cells in a total volume of 5 ml normal saline. Starting one day after infection volunteers attended
552 clinic for assessment and blood sampling every 12-hours, and parasite density was measured in
553 real time by qPCR (target gene = 18S ribosomal RNA). In VAC063A thick blood films were also
554 evaluated at each time-point by experienced microscopists and diagnosis required volunteers to fulfil
555 two out of three criteria: a positive thick blood film (one viable parasite in 200 fields) and/or qPCR
556 data showing at least 500 parasites per ml and/or symptoms consistent with malaria. In VAC063B
557 and C microscopy was removed as a diagnostic tool to reduce the number of volunteers diagnosed
558 prematurely without impacting volunteer safety. The new criteria for diagnosis were: asymptomatic
559 with any available qPCR result above 10,000 parasites per ml or symptomatic with any available
560 qPCR data above 5000 parasites per ml. At diagnosis volunteers were treated with artemether and
561 lumefantrine (Riamet) except in cases where its use was contraindicated and atovaquone and
562 proguanil (Malarone) were given instead. In our analysis, we refer to the blood-draw immediately
563 before drug-treatment as the diagnosis time-point.

564 Clinical symptoms of malaria (pyrexia, malaise, fatigue, arthralgia, back pain, headache, myalgia,
565 chills, rigor, sweats, headache, nausea, vomiting and diarrhoea) were either recorded by the

566 volunteers on diary cards or during clinic visits. All symptoms were recorded as adverse events and
567 assigned a severity score: 0 - absent; 1 - transient or mild discomfort (no medical intervention
568 required); 2 - mild to moderate limitation in activity (no or minimal medical intervention required); 3 -
569 severe limitation in activity requiring assistance (may require medical intervention). Pyrexia was
570 scored as follows: absent (≤ 37.5°C), mild (37.6 - 38.2°C), moderate (38.3 - 38.9°C) and severe (≥
571 39°C). In addition, full blood counts and blood chemistry were evaluated at the Churchill and John
572 Radcliffe Hospital in Oxford providing 5-part differential white cell counts and quantification of
573 electrolytes, urea, creatinine, bilirubin, alanine aminotransferase (ALT), alkaline phosphatase (ALP)
574 and albumin.

575 **Meta-analysis of liver injury**

576 A surrogate dataset from Reuling *et al.* (33) was used to assess the risk of liver injury during a first-
577 in-life infection compared to re-challenge. We extracted data from every CHMI study that used the
578 3D7 *P. falciparum* clone (or its parental NF54 line), initiated infection via mosquito bite or direct blood
579 challenge and that had a treatment threshold based on thick smear positivity (estimated to be at
580 least 5,000 parasites per ml). This produced data for 95 volunteers across 7 CHMI studies. Notably,
581 Reuling *et al.* used longitudinal data to show that liver function test (LFT) abnormalities peaked up
582 to 6-days post-treatment in line with our own T6 time-point. And furthermore, in every CHMI study
583 (including our own) LFT abnormalities were graded using the same adaptation of the WHO adverse
584 event grading system. An LFT reading > 1.0 but < 2.5 times the upper limit of normal was graded as
585 mild; a reading > 2.5 but < 5.0 times the upper limit was graded moderate; and a reading > 5.0 the
586 upper limit was graded severe. For ALT, the upper limit of normal was 35 or 45 units per litre for
587 female and male volunteers, respectively. Data from the 95 volunteers in Reuling *et al.* and the 3
588 primary controls in our VAC063C study were pooled for analysis and we calculated a weighted peak
589 parasite density across the entire cohort by using **a**, the mean number of parasites per ml and **b**, the
590 number of volunteers in each of the 8 CHMI studies. To statistically test whether an abnormal ALT
591 reading was more prevalent in the 98 volunteers experiencing their first malaria infection compared
592 to the 8 volunteers undergoing re-challenge (either second or third infection) we used Barnard's test,
593 which examines the association of two independent categorical variables in a 2x2 contingency table.
594 A p value below 0.05 was considered significant.

595 **Processing whole blood for RNA and plasma**

596 Venous blood was drawn into K_2EDTA-coated vacutainers (Becton Dickinson #367835). To preserve
597 RNA for whole blood transcriptome analysis 1 ml of blood was mixed thoroughly with 2 ml Tempus
598 reagent (ThermoFisher #4342792) and samples were stored at -80°C. Note that no more than 2-
599 hours passed between blood draw and RNA preservation. To obtain platelet-depleted plasma 3 ml
600 of blood was divided into two 2 ml Eppendorf tubes and centrifuged at 1,000 xg for 10-minutes at
601 4°C to pellet cellular components. Working on ice, plasma was then carefully transferred to a new
602 tube and spun again – this time at 2,000 xg for 15-minutes at 4°C to pellet platelets. Cell-free,
603 platelet-depleted plasma was then aliquoted into new tubes, snap frozen on dry ice and stored at -
604 80°C.

605 **Whole blood RNA-sequencing**

606 Whole blood RNA was extracted using the Tempus Spin RNA isolation reagent kit (ThermoFisher
607 #4380204) according to the manufacturer's instructions. To account for the reduced starting volume
608 and to maintain Tempus stabilizing reagent at the correct final concentration we added just 1 ml PBS
609 to each sample after thawing. Diluted samples were then centrifuged at 3000 xg for 30-minutes at
610 4°C to pellet nucleic acids. Pellets were resuspended in RNA purification resuspension solution and
611 centrifuged on a silica column to remove non-nucleic acid contaminants. After washing, the column
612 was incubated for 2-minutes at 70°C before eluting nucleic acids. 40 μl eluate was then subjected to
613 DNA digestion using the RNA Clean and Concentrator-5 kit (Zymo Research #R1013). Purified RNA
614 was eluted in 30 μl DNAse/RNAse-free water, quantified using a Qubit Fluorometer (HS RNA assay
615 kit, ThermoFisher #Q32852) and RNA integrity assessed using an Agilent Bioanalyzer 2100 (RNA
616 6000 nano kit Agilent #5067-1511). The average RNA integrity number (RIN) was 9 (98% of samples
617 > 8, lowest RIN 7). Libraries were prepared by Edinburgh Genomics (Edinburgh, UK) using the
618 TruSeq Stranded mRNA library prep kit (Illumina #20020595). Stranded library preparation allows
619 transcript expression to be estimated more accurately; in particular it is more effective in quantifying
620 anti-sense gene expression, properly assigning transcripts to putative coding genes and to resolve
621 ambiguity in reads from overlapping genes. Libraries were sequenced using the NovaSeq 6,000
622 Illumina platform yielding 50 bp paired end (PE) reads. These short reads are sufficient to accurately
623 capture gene expression thanks to the well annotated human transcriptome. The average number
624 of reads per sample passing QC across all samples was 8.45×10^7.

625 **Data analysis of whole blood RNA-sequencing**

626 Quality and content of FASTQ files, which contain raw PE sequencing reads, were assessed using
627 FastQC (http://www.bioinformatics.babraham.ac.uk/projects/fastqc). A single sample (volunteer
628 1040 baseline second infection) failed quality control and we therefore excluded all RNAseq data
629 from this volunteer's second infection from our analysis. TruSeq primer sequences were removed
630 using cutadapt v1.9, reads were aligned to the Ensembl release 96 Homo sapiens transcript set with
631 bowtie2 v2.2.7 (49) (parameters: —very-sensitive -p 30 —no-mixed —no-discordant —no-unal) and
632 reads that mapped to globin transcripts were discarded (on average 11.7% of mapped reads, range
633 1.6 – 38.1%). We opted for bioinformatic globin depletion as it is highly sensitive and reproducible
634 (50) whereas depleting globin during RNA preparation can compromise the amount and quality of
635 RNA recovered (51). Following these steps, the average alignment rate to the human transcriptome
636 across all samples was 88%. A matrix of normalised counts for each transcript was obtained from
637 sorted, indexed bam files using samtools idxstats (http://www.htslib.org/doc/samtools.html).
638 Transcript counts were imported into the R/Bioconductor environment (v3.6) and differential gene
639 expression analyses (pairwise group comparisons) performed using functions within the DESeq2
640 package (52). lfcShrink was applied to the output of each pairwise comparison (type normal). Lists
641 of differentially expressed transcripts were analysed using R (v3.6) - non-coding transcripts were
642 removed and multiple transcripts annotated to the same gene were consolidated by keeping the
643 transcript with the highest absolute fold-change. Only protein-coding transcripts with an adjusted p
644 value (adj p) < 0.05 and a fold-change > 1.5 were considered differentially expressed. Radar plots
645 and heatmaps were generated using the *ggplot2* package (53). The genelists used for cell cycle
646 analysis were manually compiled from published datasets (54, 55) and we allocated genes to a
647 single phase based on cell cycle transcriptional network analysis (56, 57).

648 **Flow-sorting CD4$^+$ T cells**

649 We flow-sorted CD4$^+$ T cell subsets for *ex vivo* RNA-sequencing from 3 ml whole blood collected in
650 K_2EDTA Vacutainers. After red cell lysis (erythrocyte lysis buffer, ebioscience #00-4300-54)
651 leukocytes were washed in flow buffer (PBS supplemented with 2% fetal bovine serum (FBS
652 Performance Plus, ThermoFisher #16000044, heat inactivated & filtered 0.22 µm) and 5 mM EDTA
653 (Life Technologies #AM9260G)). We then blocked Fc receptors (human TruStain FcX, BioLegend
654 #422302) and stained leukocytes for 20-minutes at 4°C (8-colour panel: CD3 (clone OKT3), CD4
655 (clone OKT4), CD127 (clone A019D5), CD25 (clone M-A251), CCR7 (clone G043H7), CD45RA
656 (clone HI100), CD38 (clone HIT2) and HLA-DR (clone L243)). After washing leukocytes were kept
657 in cold flow buffer and filtered through a 40 µm cell strainer (Scientific Labs Supply #352340). We
658 used a FACS-Aria IIIu or Fusion cell sorter (BD Biosciences, FACS Diva v8 software, 70 µm nozzle,
659 sort setting "purity") to simultaneously sort 10,000 of each of the following CD4$^+$ T cell subsets -
660 naive (CD3^{pos} CD4^{pos} CD127^{pos} CCR7^{pos} CD45RA^{pos}), effector/effector memory (EM) (CD3^{pos} CD4^{pos}
661 CD127^{pos} CCR7^{neg} CD45RA^{neg}) and regulatory (CD3^{pos} CD4^{pos} CD25^{hi} CD127^{neg}). T cells were sorted
662 directly into RNAse free sterile 1.5 ml screw cap tubes (ThermoFisher #11529924) containing 1 ml
663 Trizol Reagent (ThermoFisher #15596026). Tubes were incubated for 5-minutes at room
664 temperature and stored at -80°C. At the same time, we sorted naive T cells into flow buffer and
665 reacquired them to check sort purity, which was above 95% for every sample analysed in this study.
666 Flow data acquired during sorting was analysed using FlowJo v9 software.

667 **CD4$^+$ T cell RNA-sequencing**

668 RNA was extracted using a modified phenol-chloroform protocol (58) with 1-Bromo-3-chloropropane
669 (Sigma-Aldrich #B62404) and Isopropanol (Acros Organics #423835000). Total RNA was quantified
670 and assessed for quality and integrity by Bioanalyser (RNA Pico 6000 Chip, Agilent #5067-1513) -
671 all sequenced samples had a RIN value above 8. cDNA was generated from 1 ng total RNA using
672 the SMART-Seq v4 Ultra Low Input RNA Kit (Takara Bio #634894) and amplified using 12 cycles of
673 PCR. Amplified cDNA was purified using Agencourt AMPure XP beads (Beckman Coulter #A63880),
674 quantified on a Qubit Fluorometer (dsDNA HS assay kit, ThermoFisher #Q32851) and quality
675 assessed by Bioanalyser (DNA HS Kit, Agilent #5067-4626). Libraries were then constructed from
676 150 pg of cDNA using the Nextera XT DNA Library Preparation Kit (Illumina #FC-131-1024)
677 according to the manufacturer's instructions. Libraries were quantified by Qubit (dsDNA HS assay)
678 and fragment size distribution was assessed by Bioanalyser (DNA HS Kit). Using this information,
679 samples were combined to create equimolar library pools that were sequenced on a NextSeq 550
680 Illumina platform to yield 75 bp PE reads; the average number of PE reads per sample passing QC
681 across all samples was 2.74 x 10^7.

682 **Data analysis of CD4$^+$ T cell RNA-sequencing**

683 Quality and content of FASTQ files were assessed using FastQC and reads were aligned to the
684 Ensembl release 96 Homo sapiens transcript set with bowtie2 v2.2.7 (49) (parameters: —very-
685 sensitive -p 30 —no-mixed —no-discordant —no-unal). Our median alignment rate was 66.4% after
686 removing primer and adapter traces (SMART-Seq v4 primers, polyG, polyT and polyN) with cutadapt
687 v1.9. The sorted, indexed bam files were then used to obtain a matrix of normalised counts for each
688 transcript using samtools idxstats. Transcript counts were imported into the R/Bioconductor

689 environment (v3.6) and differential gene expression analyses (pairwise group comparisons)
690 performed using functions within the DESeq2 package (52). lfcShrink was applied to the output of
691 each comparison (type normal). Lists of differentially expressed transcripts were filtered by removing
692 all non-coding transcripts and retaining only those with adj $p < 0.05$ and fold-change > 1.5. Multiple
693 transcripts annotated to the same gene were consolidated by keeping the transcript with the highest
694 absolute fold-change. Heatmaps and circular stacked bar plots were generated using the *ggplot2*
695 package.

696 **Functional gene enrichment analysis using clueGO**

697 Lists of differentially expressed genes were imported into clueGO v2.5.7 (59, 60). ClueGO identified
698 significantly enriched GO terms (GO Biological Process and GO Molecular Function) associated with
699 these genes and placed them into a functionally organised non-redundant gene ontology network
700 based on the following parameters: adj p cutoff = 0.01; correction method used = Bonferroni step
701 down; min. GO level = 5; max. GO level = 11; number of genes = 3; min. percentage = 5.0; GO
702 fusion = true; sharing group percentage = 40.0; merge redundant groups with > 40.0% overlap;
703 kappa score threshold = 0.4; and evidence codes used [All]. Each of the functional groups was
704 assigned a unique colour and a network was then generated using an edge-weighted spring-
705 embedded layout based on kappa score. Groups were named by the leading GO term (lowest adj p
706 with min. GO level 5 or 6). Merged networks were constructed by inputting two lists of differentially
707 expressed genes. For each GO term information on what fraction of associated genes were derived
708 from each list was retained. Any GO term containing > 60% associated genes from a single list was
709 considered to be enriched in that group, otherwise GO terms were considered to be shared.

710 **Multiplexed plasma analyte analysis**

711 The concentration of 39 analytes was measured in plasma samples collected at baseline, during
712 infection, diagnosis, 6-days after drug treatment (T6) and at a memory timepoint (28- or 45-days
713 post-challenge). Plasma was thawed on ice and centrifuged at 1000 xg for 1-minute to remove
714 potential protein aggregates. We customised 4 LEGENDplex panels (BioLegend) and performed
715 each assay on filter plates according to the manufacturer's instructions. Samples and standards
716 were acquired on a LSRFortessa flow cytometer (BD Biosciences). FCS files were processed using
717 LEGENDplex software (version 7.1), which automatically interpolates a standard curve using the
718 plate-specific standards and calculates analyte concentrations for each sample. All samples from
719 v1040 were excluded after failing QC and downstream data analysis was performed in R v3.6. To
720 determine which plasma analytes varied significantly through time we used the *lme4* package to fit
721 a linear mixed-effects model for each analyte. All available time-points were included and models
722 were fitted using log2 transformed plasma analyte concentration as dependent variable, time-point
723 as a categorical fixed effect and volunteer as a random effect. A Kenward-Roger approximation was
724 used to calculate p values (using the *pbkrtest* package), which were adjusted for multiple testing
725 (Benjamini-Hochberg method). Results were visualised with *ggplot2* (53) and only those with at least
726 a 1.5 fold-change from baseline are shown. To determine which plasma analytes varied between
727 infections at diagnosis we used *lme4* to fit a mixed-effects model for each analyte in the form of
728 analyte ~ timepoint + infection_number + (1|volunteer) using log2 transformed concentrations. Time-
729 point and infection number were included as categorical fixed effects and volunteer as a random
730 effect. Linear hypothesis testing via pairwise comparisons was performed using *multcomp*'s glht

731 function and adjusted for multiple testing (Benjamini and Hochberg). Only analytes that were
732 significant in both second and third infection (versus first infection) are shown (adj $p < 0.05$ and fold-
733 change > 1.5).

734 **Pearson correlation analysis**

735 The fold-change of each significant plasma analyte (shown in figure 3 - supplement 1B), the number
736 of circulating lymphocytes and haemoglobin concentration were calculated at diagnosis or T6
737 (relative to baseline) according to their largest absolute fold-change. The percentage of activated
738 effector and regulatory $CD4^+$ T cells, the maximum parasite density and maximum core temperature
739 (at any time-point up to 48-hours post-treatment) were also included in the analysis. All data were
740 log2 transformed and Pearson correlation was performed using the corrplot function. Correlation
741 coefficients were then used for hierarchical clustering by Euclidean distance.

742 **CyTOF sample acquisition**

743 Venous blood was collected in K_2EDTA-coated vacutainers, stabilised within 30-minutes of blood
744 draw in whole blood preservation buffer (Cytodelics #hWBCS002) and stored at -80°C. For antibody
745 staining, samples were thawed at 37°C in a water bath, fixed for 15-minutes and red blood cells
746 lysed using the whole blood preservation kit (Cytodelics #hC002). Cells were permeabilised with
747 Maxpar barcode perm buffer (Fluidigm #201057) and each sample was barcoded using Cell-ID 20-
748 plex palladium barcodes (Fluidigm #201060). Samples were then pooled and stained with our T cell
749 focussed surface antibody panel (see supplementary file 3) for 30-minutes. Following washing, cells
750 were fixed and permeabilised with the Maxpar nuclear antigen staining buffer set (Fluidigm #201063)
751 and incubated with the nuclear antibody mix for 45-minutes. After washing, cells were fixed for 10-
752 minutes in 1.6% formaldehyde diluted in PBS (ThermoFisher #28906). Cells were then washed
753 again, resuspended at a concentration of 3×10^6 cells per ml in 72.5 nM Cell-ID Intercalator Ir solution
754 (Fluidigm #201192A) and stored overnight at 4°C. Samples were acquired the next day on a freshly
755 tuned Helios mass cytometer (Fluidigm, acquisition rate 300-500 events/second) using the WB
756 injector and 10% EQ Four Element Calibration Beads (140Ce, 151Eu, 165Ho, and 175Lu; Fluidigm
757 #201078).

758 **CyTOF data analysis**

759 The Fluidigm CyTOF software (version 6.7) generated FCS files, which were normalised (61) and
760 debarcoded (62) using the R package CATALYST (63). Samples were compensated using single
761 stained beads (64). After exclusion of normalisation beads and doublets we gated on $CD45^{pos}$ $CD3^{pos}$
762 T cells using the Cytobank web portal (Beckman Coulter, www.cytobank.org). We then inspected
763 the intensity distribution of each channel and removed channels of low variance (CD3, CD16, CD45,
764 CD69, CXCR5, GATA3, RORγt, TCRγδ, and Tim3). The remaining 30 markers were used for both
765 UMAP projections and FlowSOM clustering.

766 UMAP (65) was used to generate a 2D projection of this high-dimensional dataset. Here phenotypic
767 similarity of cells within and between populations is preserved in the Euclidean distance of the
768 projection. We used its R implementation in the *scater* package (66), which in turn relies on *uwot*
769 (github.com/jlmelville/uwot). Features were scaled to unit variance and the 15 nearest neighbours

were considered for embedding. UMAP coordinates were then exported for visualisation using *ggplot2* (53). FlowSOM (67) uses self-organising maps (SOM) to efficiently categorise cytometry data into non-overlapping cell populations and was performed using CATALYST (63) (default parameters, target: 100 clusters, 50 metaclusters). After manual inspection we merged two phenotypically similar clusters to avoid overclustering (68) and ended up with 49 discrete T cell clusters. The R/Bioconductor package *ComplexHeatmap* (69) was used to visualise T cell phenotypes; the arcsine transfomed signal intensity of each marker was independently scaled using a 0-1 transformation across all 49 clusters.

For differential cluster abundance analysis we used the workflow laid out by Nowicka *et al*. (70). FlowSOM cluster cell counts were modelled linearly with time-point as a dependent categorical variable and volunteer as a fixed effect using the *diffcyt* (71) implementation of edgeR (72). The edgeR functions automatically normalise cluster counts for the total number of cells and improve statistical power by sharing information on cluster count variance between clusters. Pairwise comparisons were performed relative to baseline, and clusters with an FDR < 0.05 and absolute fold change > 2 were deemed to vary significantly through time. We assessed differential cluster abundance independently for volunteers receiving either their first or third infection. We also assessed whether marker expression significantly varies through time in the major T cell subsets. To do this, we merged clusters of the same lineage according to their expression of CD4, CD8, CD56, Vδ2 and Vα7.2. $CD4^+$ and $CD8^+$ T cells were then split into naive, effector, effector memory and central memory T cells based on their expression of the markers CD45RA, CD45RO, CD57 and CCR7. All regulatory T cells ($CD25^{hi}$ $CD127^{neg}$) were merged into a single cluster as were all double negative, gamma delta, MAIT and NK T cells. Linear models derived from the *limma* package, which is optimised for continuous data, were then used to independently assess differential marker expression relative to baseline using pairwise comparisons with moderated t-tests; a shift in median expression of at least 10% and an FDR < 0.05 were required for significance. Results were visualised using *ComplexHeatmap* (69) with row-wise z-score transformed marker intensities shown for each subset.

To analyse the T cell response to *Plasmodium vivax* data from two previously conducted clinical trials were used. In VAC069A six healthy malaria-naive adults were recruited to test the infectivity and safety of a new cryopreserved stabilate containing a novel clone of *P. vivax* (PvW1); this stabilate had been carefully prepared for use in CHMI by blood challenge (Minassian *et al*., under review). In VAC069B three volunteers returned for a homologus re-challenge (8-months after VAC069A) and two additional malaria-naive adults received their first infection with PvW1. In both CHMI trials treatment was initiated once two diagnostic conditions were fulfilled: parasitaemia above 5,000 parasite genome copies per ml; parasitaemia above 10,000 genome copies per ml; positive thick blood smear and/or symptoms consistent with malaria. Treatment usually consisted of artemether and lumefantrine (Riamet) or atovaquone and proguanil (Malarone) if Riamet was contraindicated. Blood sampling, sample processing and CyTOF data analysis were all performed analogously to VAC063C. VAC069 was sponsored by the University of Oxford, received ethical approval from UK NHS Research Ethics Service (South Central - Hampshire A reference 18/SC/0577) and was registered on ClinicalTrials.gov (NCT03797989). The trial was conducted in line with the current version of the Declaration of Helsinki 2008 and conformed with the ICH Guidelines for Good Clinical Practice.

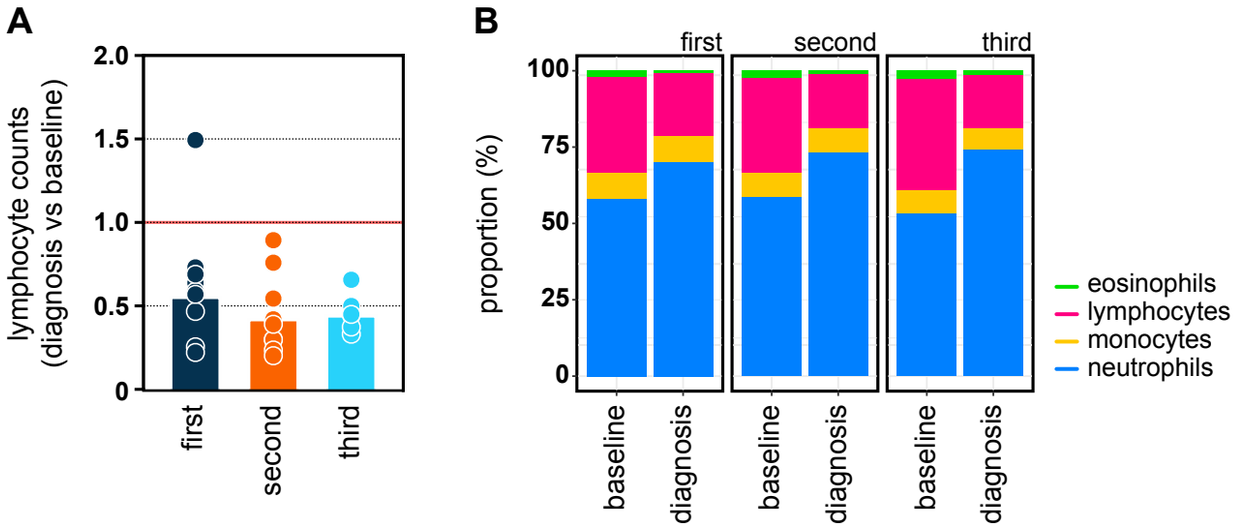

figure one - supplement 1

Figure 1 - supplement 1 | Lymphocyte recruitment to inflamed tissues is a shared response to the first three infections of life. (**A**) Lymphocytes were quantified in whole blood at diagnosis and counts were normalised to baseline measurements (taken one day before challenge). Normalised counts are shown for each volunteer (dots) and bars show the median fold-change during first, second and third infection. No statistically significant difference between infections was observed (Kruskal-Wallis test $p = 0.4483$). (**B**) Proportion of lymphocytes, monocytes, neutrophils and eosinophils in whole blood at baseline and diagnosis. The mean frequency is shown for each time-point and infection. In (A-B) $n = 10$ (first and second infection) and $n = 6$ (third infection).

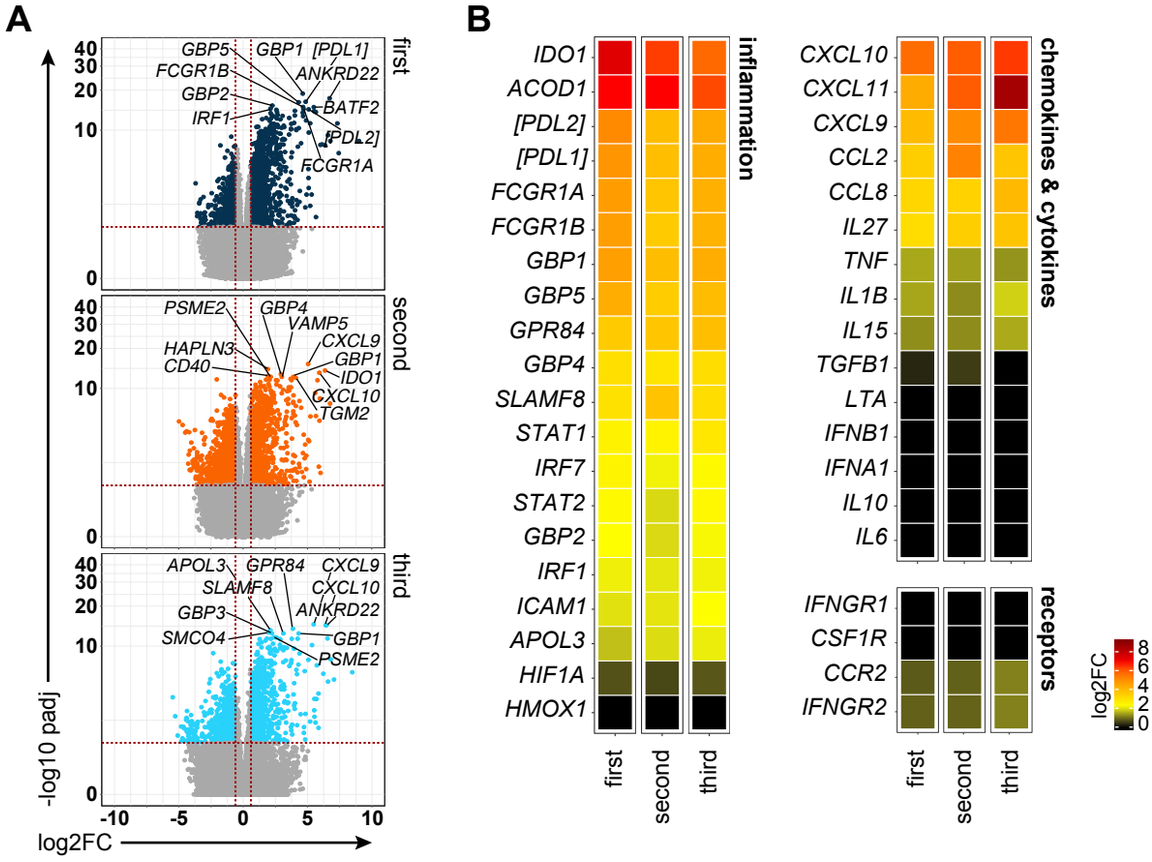

figure two - supplement 1

821 **Figure 2 - supplement 1** | Interferon-stimulated inflammation is a shared response to the first three
822 infections of life. (**A**) RNA-sequencing was used to identify differentially expressed genes in whole
823 blood at diagnosis versus baseline (adj $p < 0.05$ and > 1.5 fold-change). Note that first, second and
824 third infection were analysed independently. Volcano plots show all differentially expressed genes
825 (coloured dots) and the dashed lines represent the significance/fold-change cut-offs (genes that are
826 not significant are shown in grey). The top 10 differentially expressed genes (lowest adj p) in each
827 infection are labelled. (**B**) The log2 fold-change of signature genes associated with interferon
828 signaling and type I inflammation are shown at diagnosis (versus baseline) in first, second and third
829 infection. Square brackets indicate that common gene names have been used. In (A-B) n = 10 (first
830 infection), 9 (second infection) and 6 (third infection). v1040 was excluded from RNA-sequencing
831 analysis in second infection because their baseline sample failed QC.

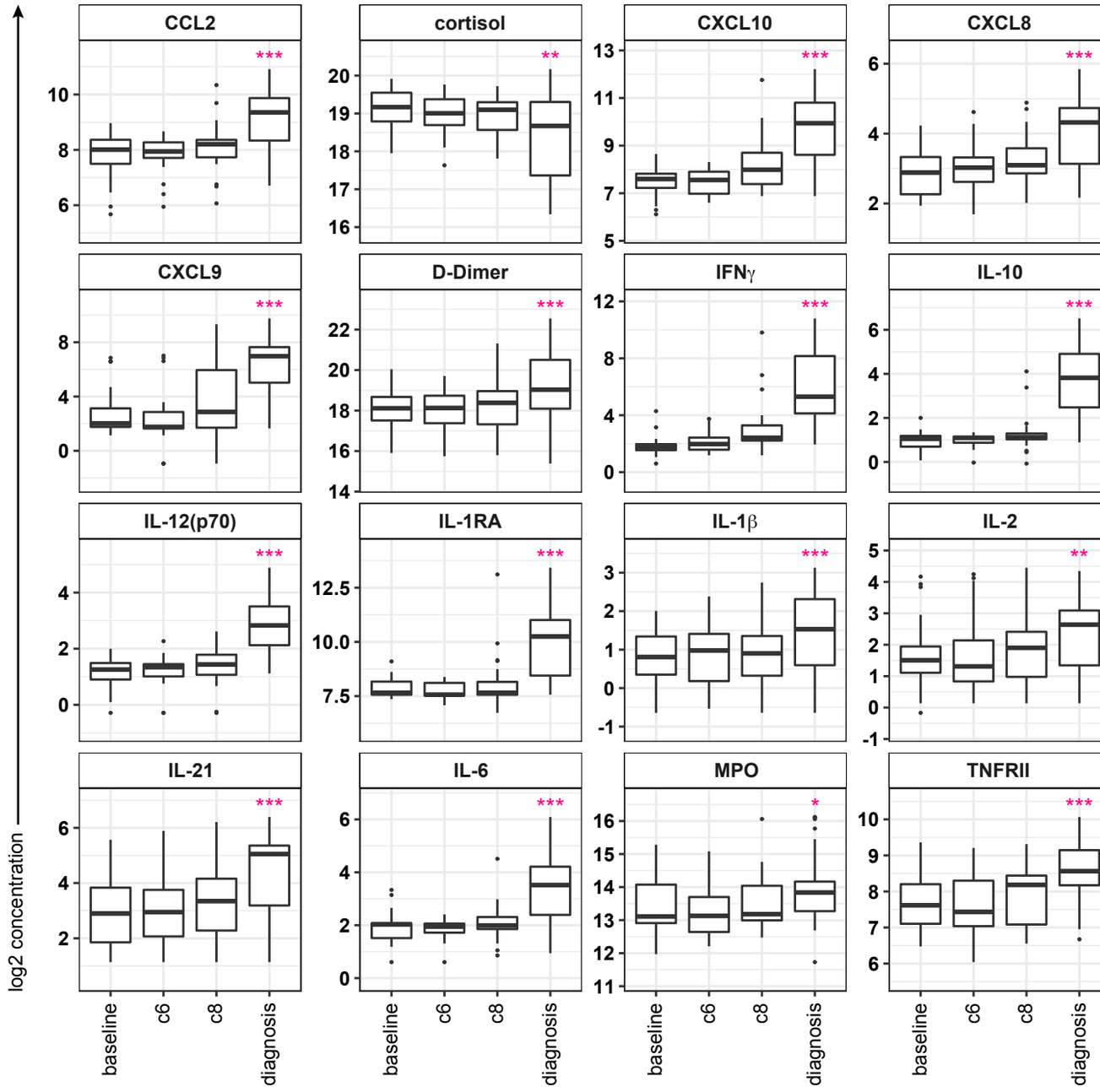

figure two - supplement 2

832 **Figure 2 - supplement 2** | Systemic inflammation peaks at diagnosis. Mixed-effects modelling was
833 used to identify plasma analytes that vary significantly at diagnosis across the entire dataset (all
834 volunteers and all infections). Kenward Roger approximation was used to calculate p values and
835 multiple test correction was performed using the Benjamini-Hochberg method (*adj $p < 0.05$, **adj p
836 < 0.005, ***adj $p < 0.0005$). Box (median and IQR) and whisker (1.5x upper or lower IQR) plots are
837 shown with outliers as dots. n = 9 (first and second infection) and 5 (third infection). v1040 was
838 excluded from plasma analysis because all samples failed QC.

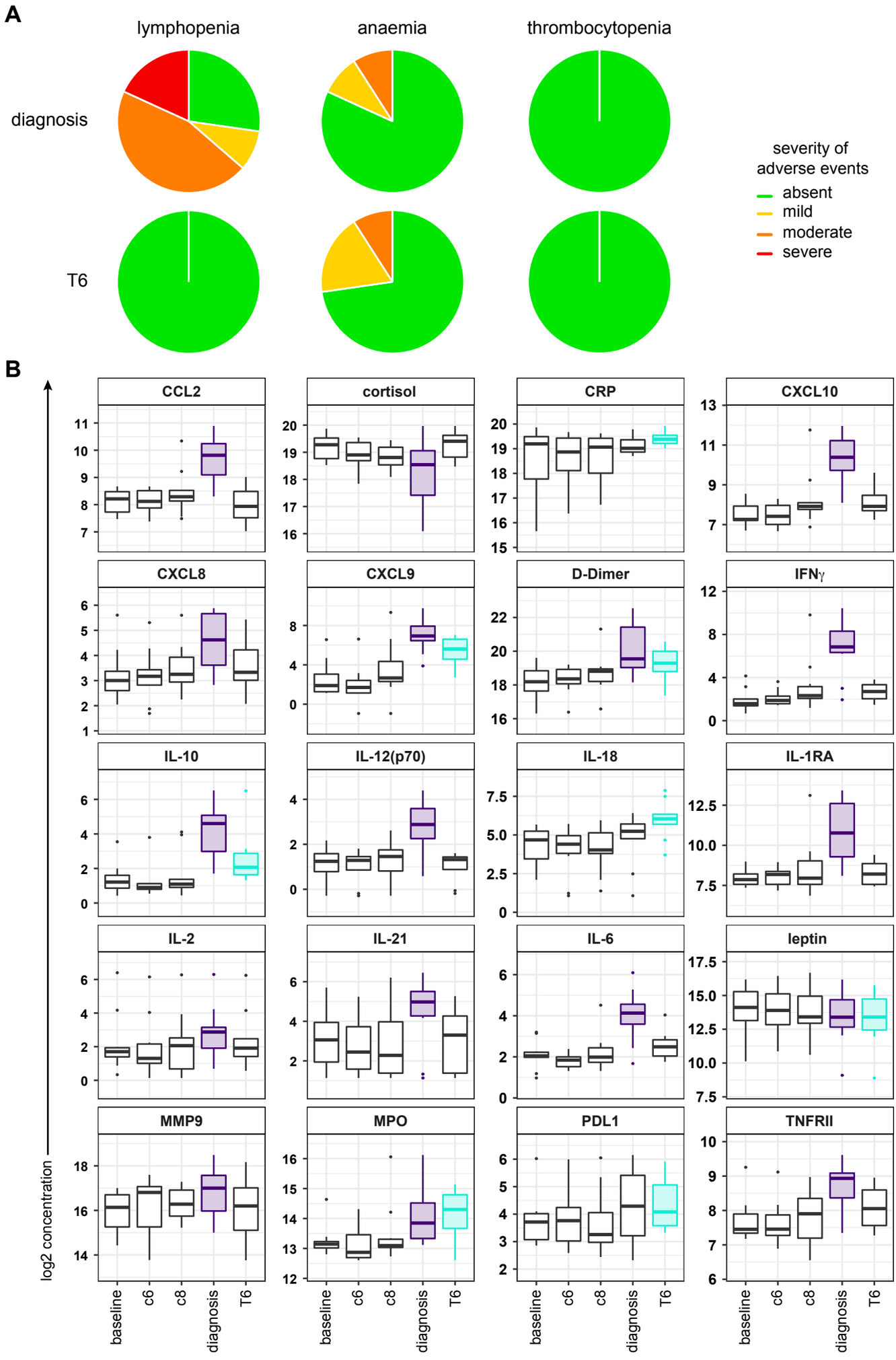

figure three - supplement 1

839 **Figure 3 - supplement 1** | The acute phase response resolves 6-days after parasite clearance. (**A**)
840 Frequency and severity of lymphopenia, anaemia and thrombocytopenia at diagnosis and T6 across
841 the VAC063C cohort. (**B**) Mixed-effects modelling was used to identify plasma analytes that vary
842 significantly at diagnosis and/or T6 across the entire dataset (all volunteers regardless of infection
843 number). Kenward Roger approximation was used to calculate p values and multiple test correction
844 was performed using the Benjamini-Hochberg method; significance (adj $p < 0.05$) is indicated by a
845 coloured box and whiskers (purple at diagnosis and turquoise at T6). In (A) n = 11 (3 first infection,
846 2 second infection and 6 third infection) and in (B) n = 10 (3 first infection, 2 second infection and 5
847 third infection). v1040 was excluded from plasma analysis because all samples failed QC.

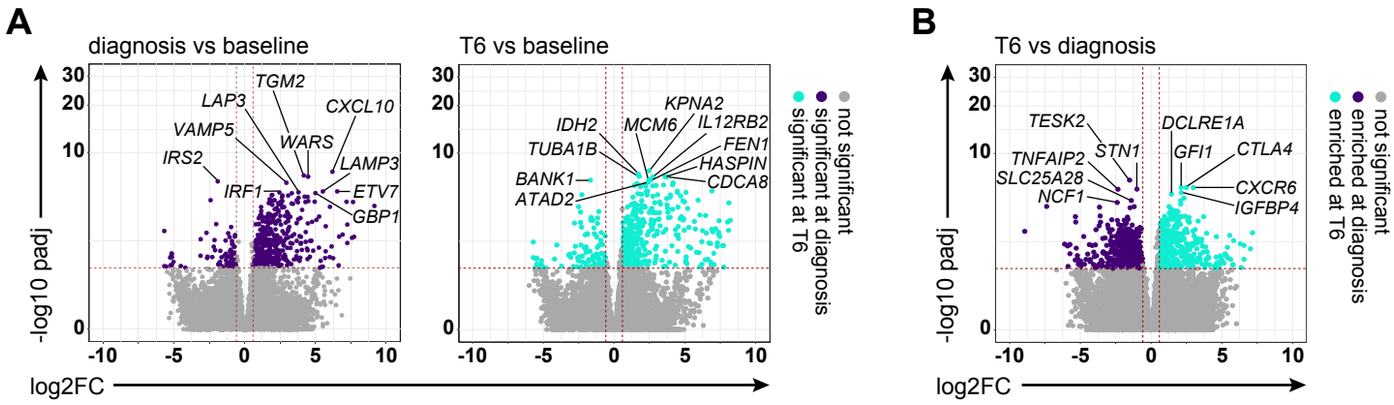

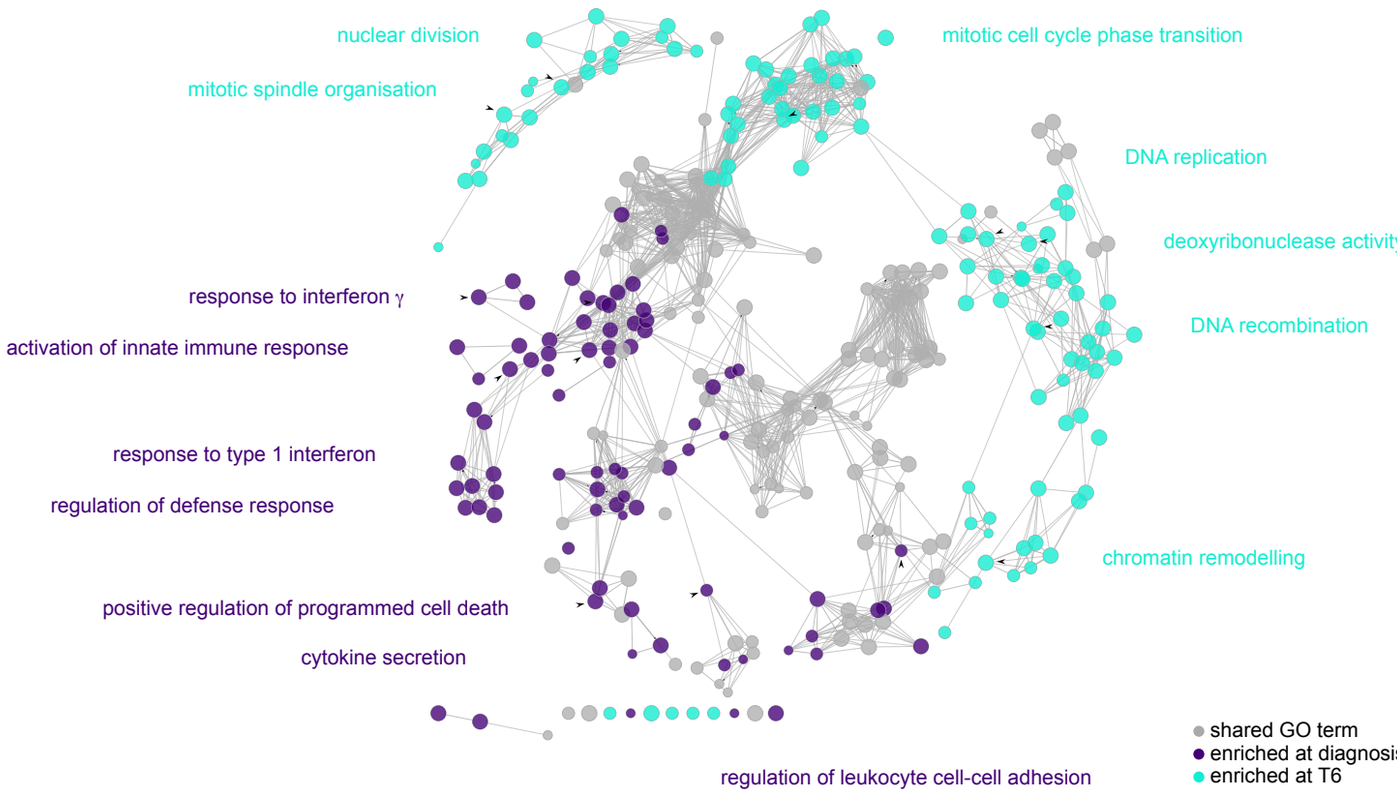

figure three - supplement 2

848 **Figure 3 - supplement 2** | The transcriptional signature in whole blood at T6 does not overlap with
849 diagnosis. (**A**) RNA-sequencing was used to identify differentially expressed genes in whole blood
850 at diagnosis (left) and T6 (right) during first infection (versus baseline, adj $p < 0.05$ and > 1.5 fold-
851 change). Volcano plots show all differentially expressed genes (coloured dots) and the dashed lines
852 represent the significance/fold-change cut-offs (genes that are not significant are shown in grey).
853 The top 10 differentially expressed genes (lowest adj p) at each time-point are labelled. (**B**) Direct
854 pairwise comparison between T6 and diagnosis - the 5 genes with the lowest adj p value are labelled
855 in both directions. (**C**) Differentially expressed genes at T6 and diagnosis were combined for GO
856 analysis of first infection and clueGO was used to construct a merged functional gene ontology
857 network. Each node represents a GO term and nodes are coloured according to whether their
858 associated genes were majoritively (> 60%) derived from the diagnosis or T6 time-point. GO terms
859 that were shared between time-points are coloured grey (see methods). Seven leading GO terms
860 (each from a unique functional group) are labelled for each time-point. In (A-C) n = 3 (all first
861 infection).

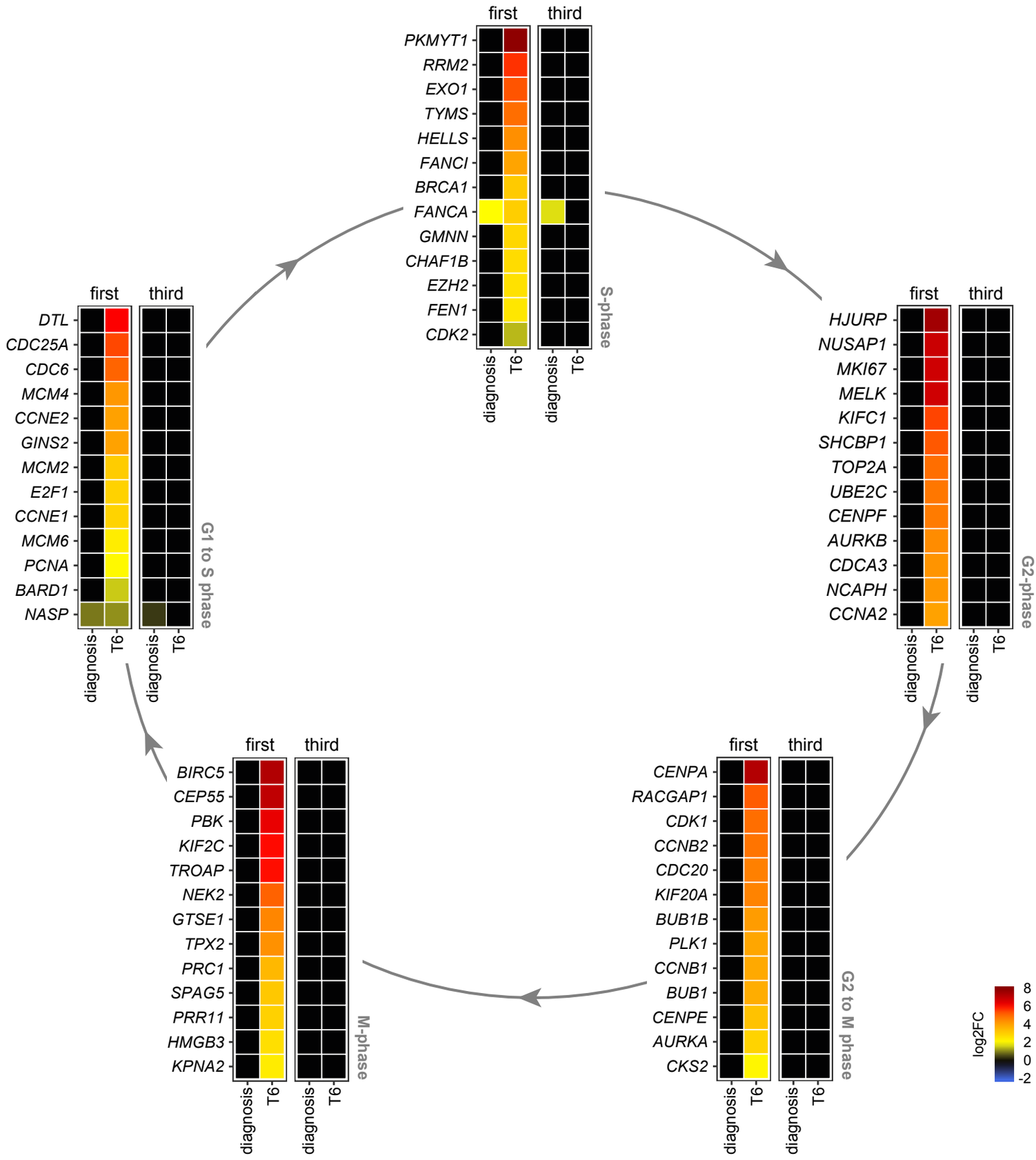

figure three - supplement 3

862 **Figure 3 - supplement 3** | The acute phase response is followed by a signature of cell proliferation
863 in naive hosts. Whole blood RNA-sequencing was used to identify differentially expressed genes at
864 diagnosis and T6 (versus baseline) during first and third infection (adj $p < 0.05$ and > 1.5 fold-
865 change). The log2 fold-change of key genes associated with each phase of the cell cycle is shown.
866 n = 3 (first infection) and 6 (third infection).

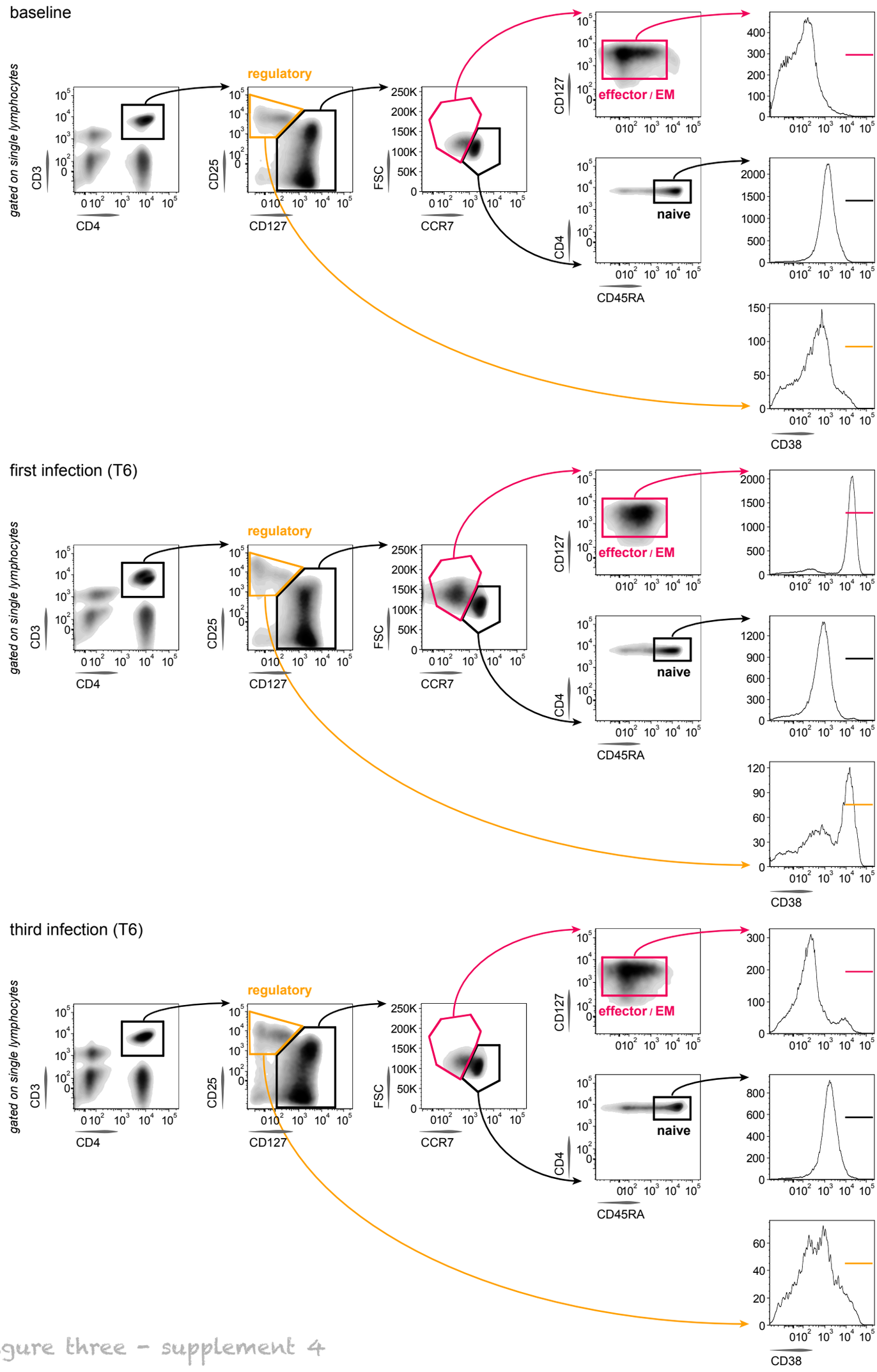

figure three - supplement 4

867 **Figure 3 - supplement 4** | Gating strategy for sorting $CD4^+$ T cells during the VAC063C trial. $CD4^+$
868 T cell subsets were sorted *ex vivo* (within 2-hours of blood draw) into TRIzol for downstream RNA-
869 sequencing - cells with a naive, effector/effector memory (EM) and regulatory phenotype were gated
870 as shown at baseline and T6. Note that we did not use CD38 for sorting but subsequently used this
871 marker to assess the level of activation within each subset at both time-points.

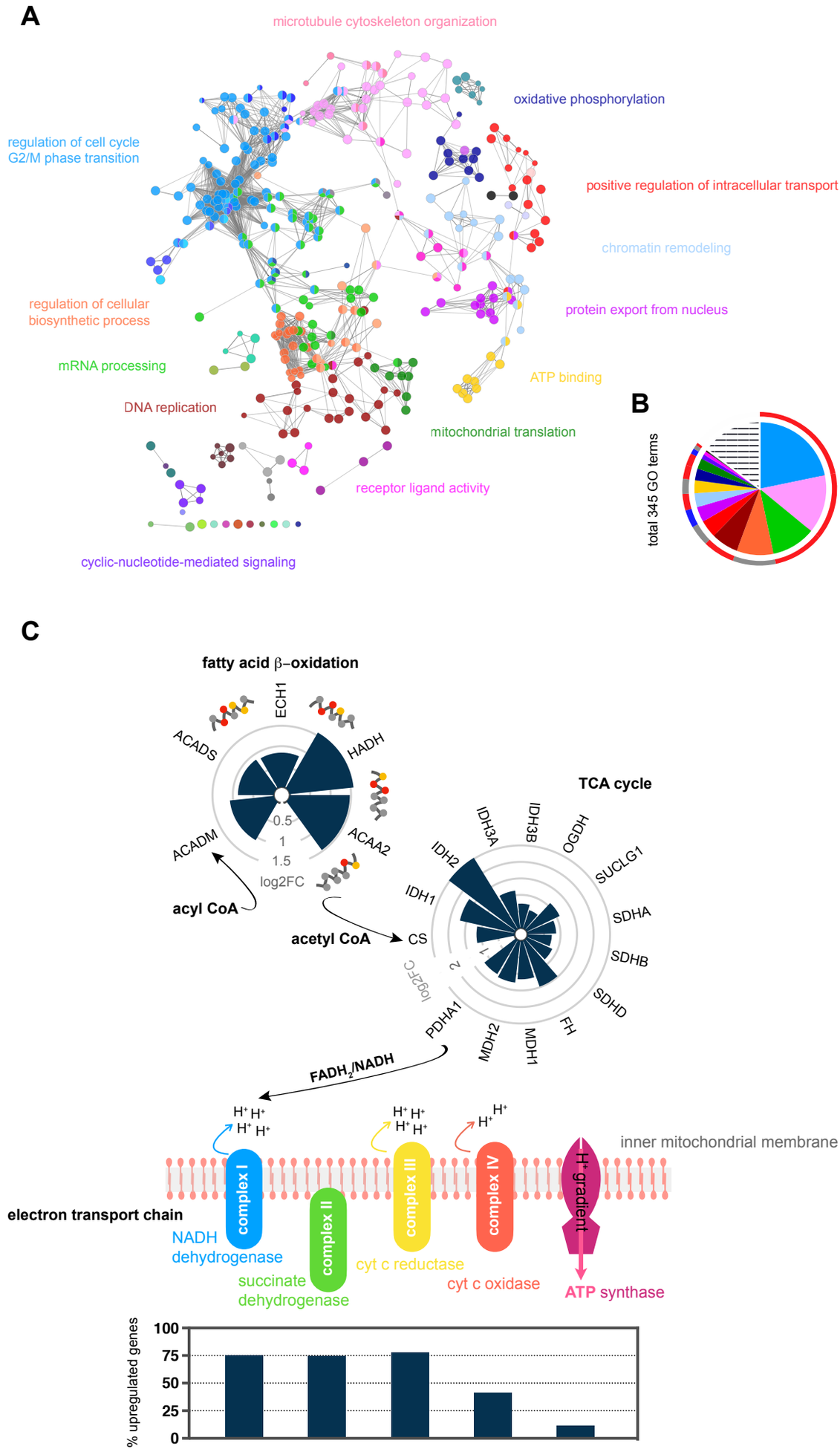

figure four - supplement 1

Figure 4 - supplement 1 | Effector $CD4^+$ T cells are proliferative and metabolically reprogrammed during first infection. (**A**-**B**) Genes that were differentially expressed in effector/effector memory (EM) $CD4^+$ T cells at T6 of first infection (versus baseline, adj $p < 0.05$ and fold-change > 1.5) were used to create a non-redundant functional gene ontology network in clueGO. Each node represents a GO term and node size is determined by adj p. Related GO terms that share > 40% of genes are connected by a line and organised into functional groups (each given a unique colour). The leading GO term from each of the 13 largest groups is labelled and (B) shows their proportion of total GO terms. The outer ring on the pie indicates whether groups were up- or downregulated (red or blue, respectively). (**C**) Transcriptional regulation of fatty acid β-oxidation, the tricarboxylic acid (TCA) cycle and oxidative phosphorylation (oxphos) in effector/EM $CD4^+$ T cells during first infection. The circular bar charts show the log2 fold-change of each major enzyme involved in fatty acid β-oxidation and the TCA cycle at T6 (shown in reaction order, clockwise). The vertical bar chart shows the proportion of oxphos enzymatic subunits that are transcriptionally upregulated at T6 - all subunits required to form complex I to IV in the electron transport chain and ATP synthase are shown. The key molecules that connect these metabolic pathways are labelled. In (A-C) n = 2 for T6 and 3 for baseline (v313 was excluded at T6 because this sample failed QC).

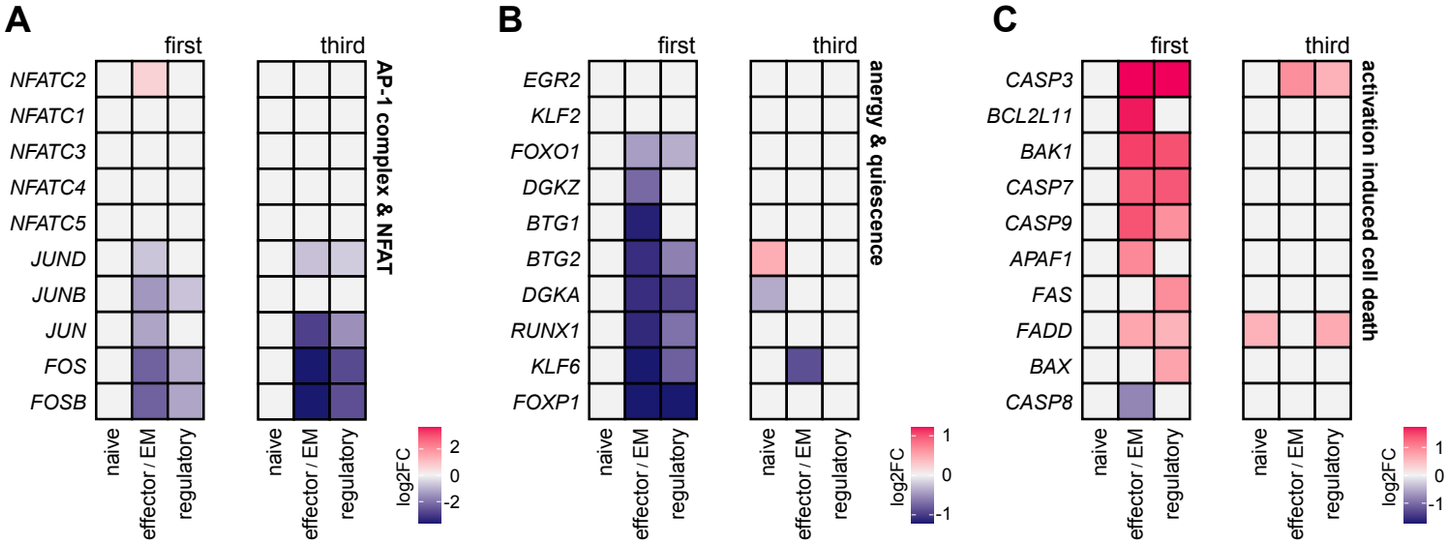

figure four - supplement 2

888 **Figure 4 - supplement 2** | $CD4^+$ T cells are not anergic, exhausted or deleted in tolerised hosts. (**A-**
889 **C**) RNA-sequencing was used to identify differentially expressed genes in naive, effector / effector
890 memory (EM) and regulatory $CD4^+$ T cells 6-days after parasite clearance (T6 versus baseline) in
891 first and third infection (adj $p < 0.05$ and > 1.5 fold-change). Heatmaps show the log2 fold-change of
892 (A) transcription factors downstream of T cell receptor signaling, (B) hallmark genes indicating T cell
893 anergy or quiescence and (C) markers of clonal deletion. In (A-C) n = 2 or 3 for first infection (T6
894 and baseline, respectively) and 6 for third infection. v313 was excluded at T6 because this sample
895 failed QC.

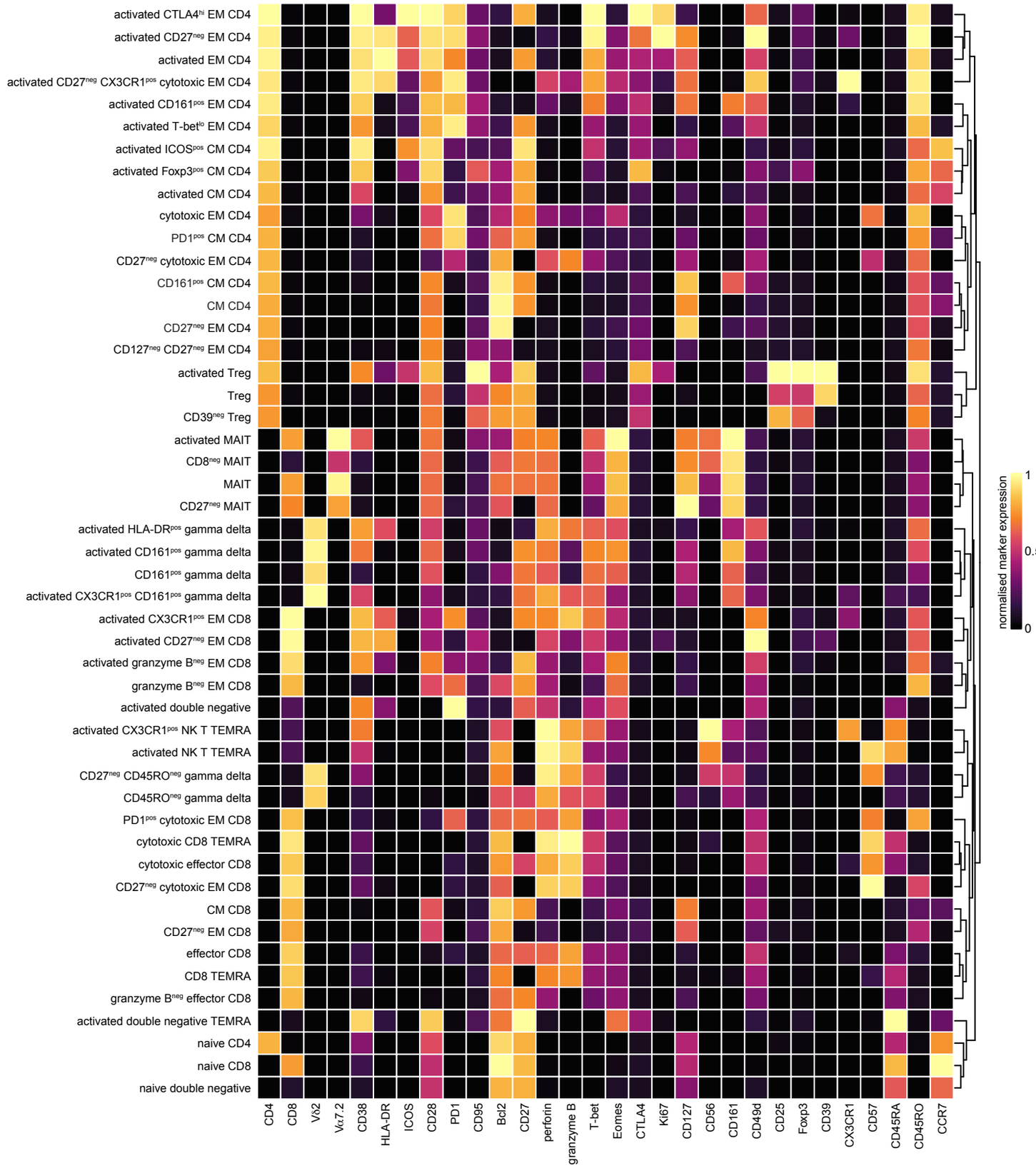

figure five - supplement 1

896 **Figure 5 - supplement 1** | Phenotype of T cell clusters. Heatmap showing the normalised median
897 expression values of all markers used for clustering in each of the 49 T cell clusters. Names were
898 assigned manually using activation, lineage and memory markers to broadly categorise each T cell
899 cluster; when more than one cluster was placed into the same category (e.g. activated EM CD4)
900 clusters were given an accessory label to highlight their unique phenotype or property (e.g. T-bet^{lo}).

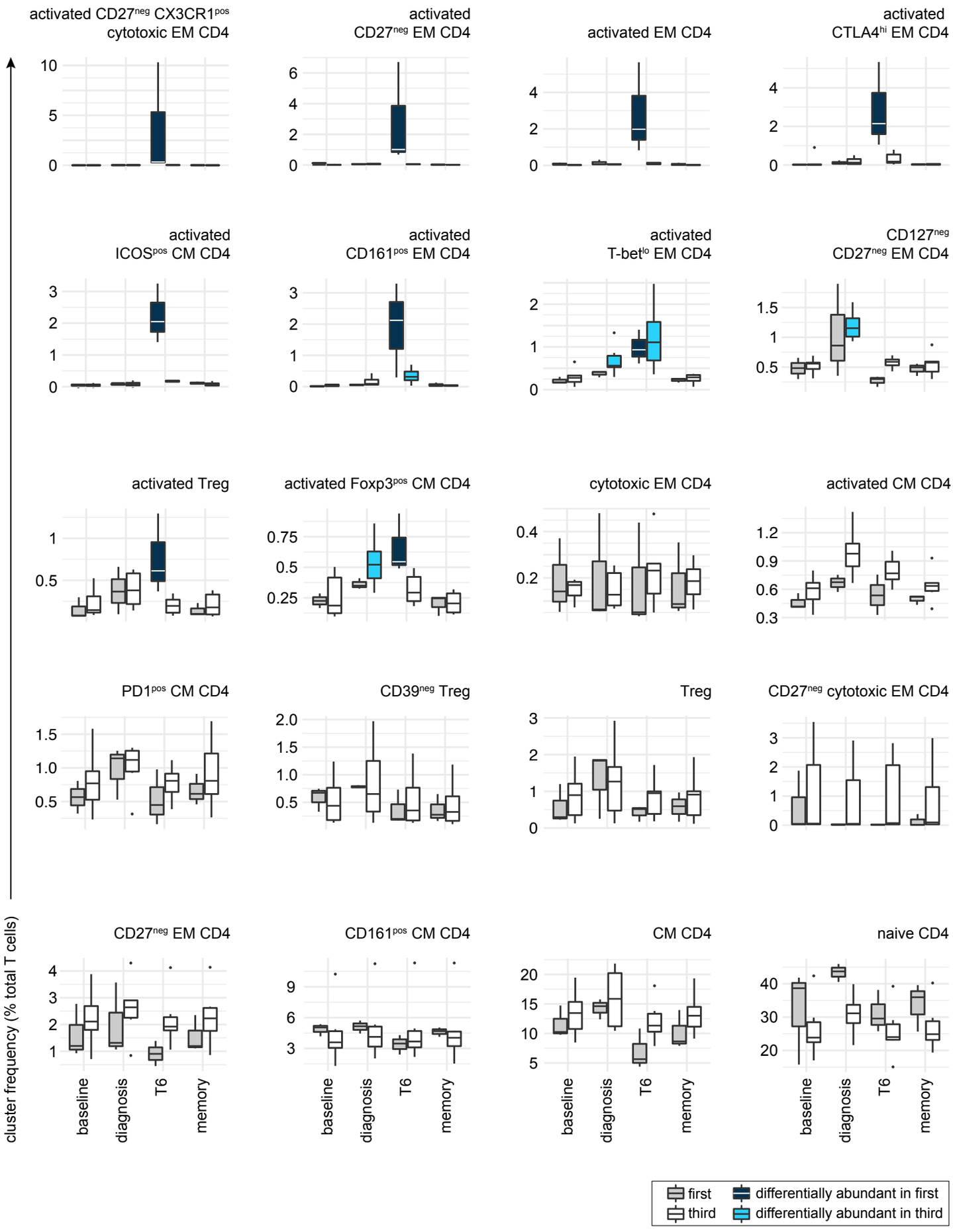

figure five - supplement 2

901 **Figure 5 - supplement 2** | Frequency of each $CD4^{+}$ T cell cluster during and after infection. Every
902 cluster is shown as a proportion of all $CD45^{pos}$ $CD3^{pos}$ T cells at each time-point. Clusters that were
903 differentially abundant in first and/or third infection are shown first (ordered by size, big to small) and
904 clusters that did not vary significantly through time are displayed thereafter (ordered by size, small
905 to big). Box (median and IQR) and whisker (1.5x upper or lower IQR) plots are shown (with outliers
906 as dots) and significance (FDR < 0.05 and > 2 fold-change) is indicated by a coloured box. $n = 3$
907 (first infection) and 6 (third infection).

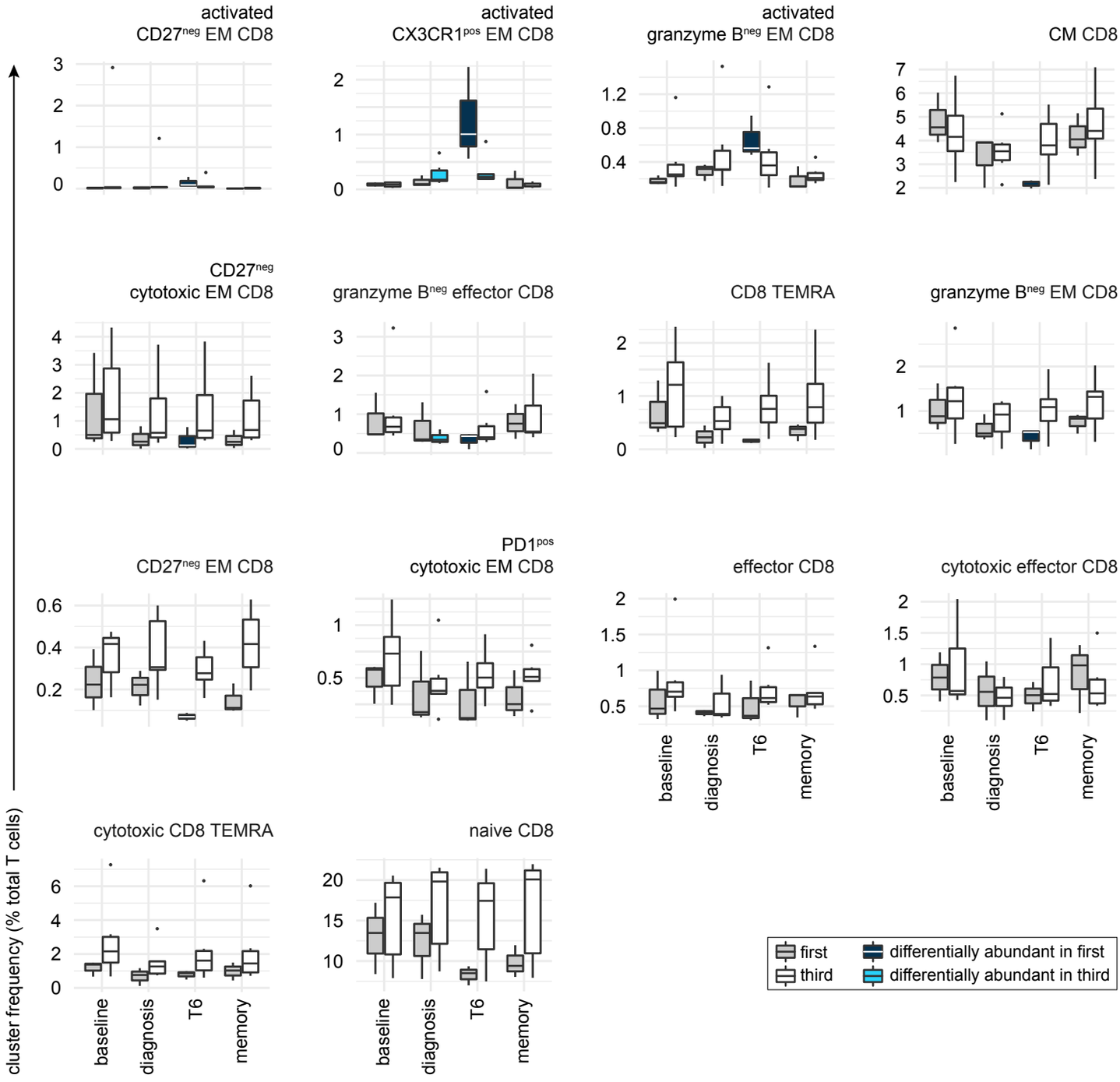

figure five - supplement 3

908 **Figure 5 - supplement 3** | Frequency of each $CD8^+$ T cell cluster during and after infection. Every
909 cluster is shown as a proportion of all $CD45^{pos}$ $CD3^{pos}$ T cells at each time-point. Clusters that were
910 significantly increased during infection are shown first followed by clusters that were significantly
911 decreased (ordered by size, big to small). Thereafter, clusters that did not vary significantly through
912 time are displayed (ordered by size, small to big). Box (median and IQR) and whisker (1.5x upper or
913 lower IQR) plots are shown (with outliers as dots) and significance (FDR < 0.05 and > 2 fold-change)
914 is indicated by a coloured box. n = 3 (first infection) and 6 (third infection).

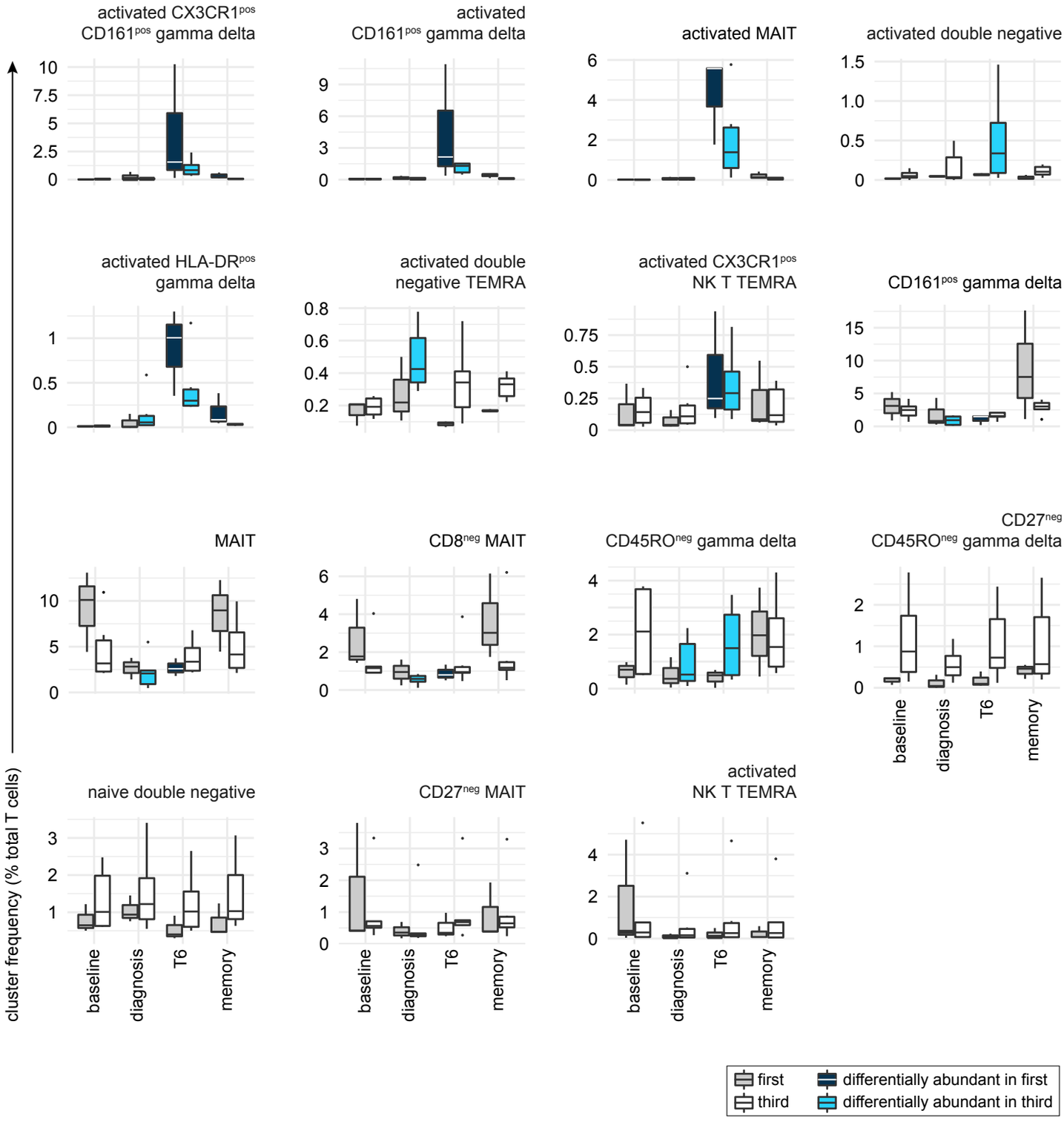

figure five - supplement 4

Figure 5 - supplement 4 | Frequency of each innate-like T cell cluster during and after infection. Every cluster is shown as a proportion of all $CD45^{pos}$ $CD3^{pos}$ T cells at each time-point. Clusters that were significantly increased during infection are shown first followed by clusters that were significantly decreased (ordered by size, big to small). Thereafter, clusters that did not vary significantly through time are displayed (ordered by size, small to big). Box (median and IQR) and whisker (1.5x upper or lower IQR) plots are shown (with outliers as dots) and significance (FDR < 0.05 and > 2 fold-change) is indicated by a coloured box. n = 3 (first infection) and 6 (third infection).

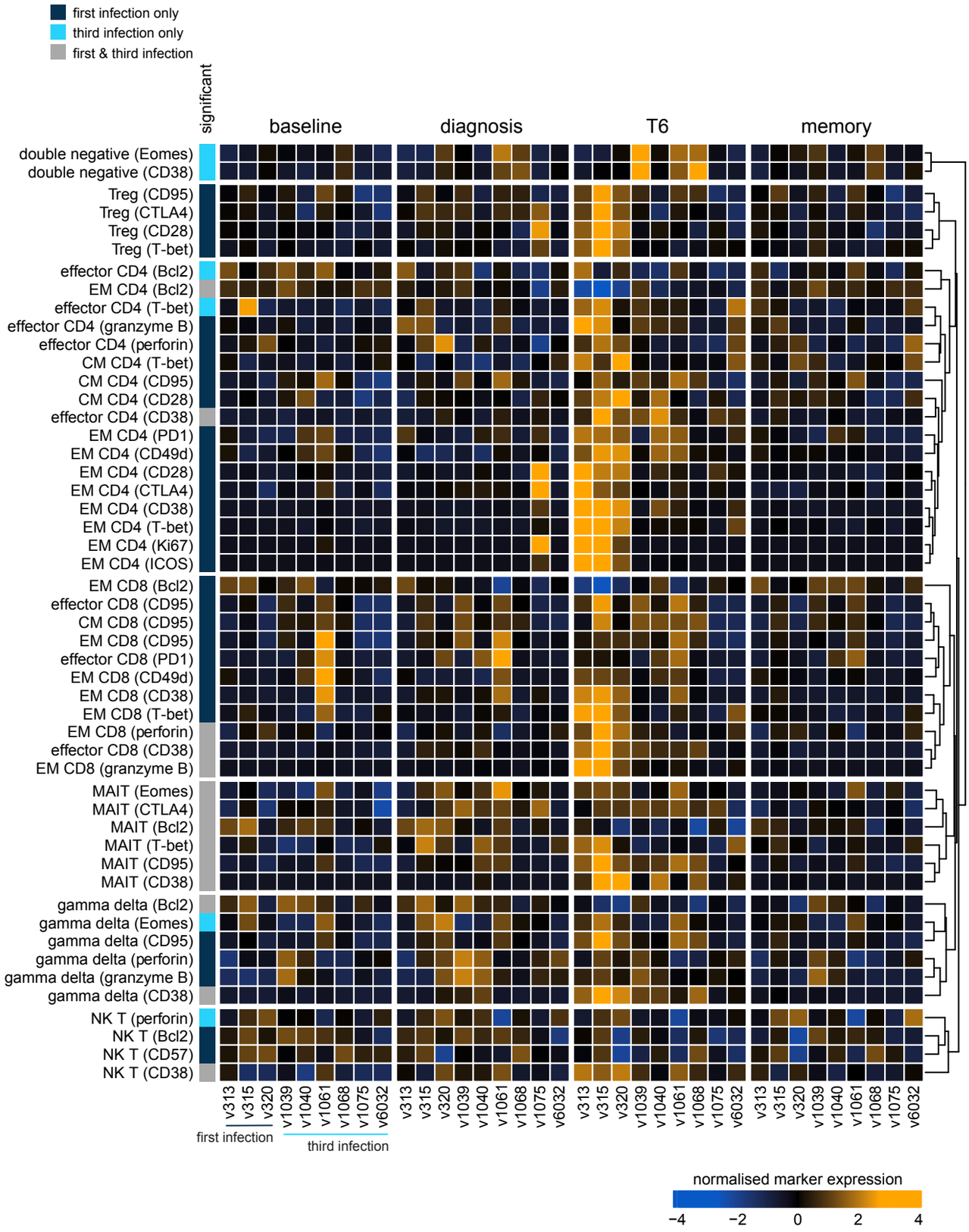

figure five - supplement 5

Figure 5 - supplement 5 | Differential marker expression reveals attenuation of the adaptive T cell response to re-challenge. We assessed whether marker expression significantly varies through time in all major T cell subsets. First, T cell clusters belonging to the same lineage were merged and then $CD4^+$ and $CD8^+$ T cells were split into naive, effector, effector memory (EM) and central memory (CM) subsets. Next, linear models were used to independently assess differential marker expression in each subset at each time-point (relative to baseline); a shift in median expression of at least 10% and an FDR < 0.05 were required for significance. Shown are all subset/marker pairs that were called as significant at T6 and data are presented as row-wise z-score marker intensities. Colour codes to the left of the heatmap indicate whether markers were differentially expressed during first infection, third infection or both infections.

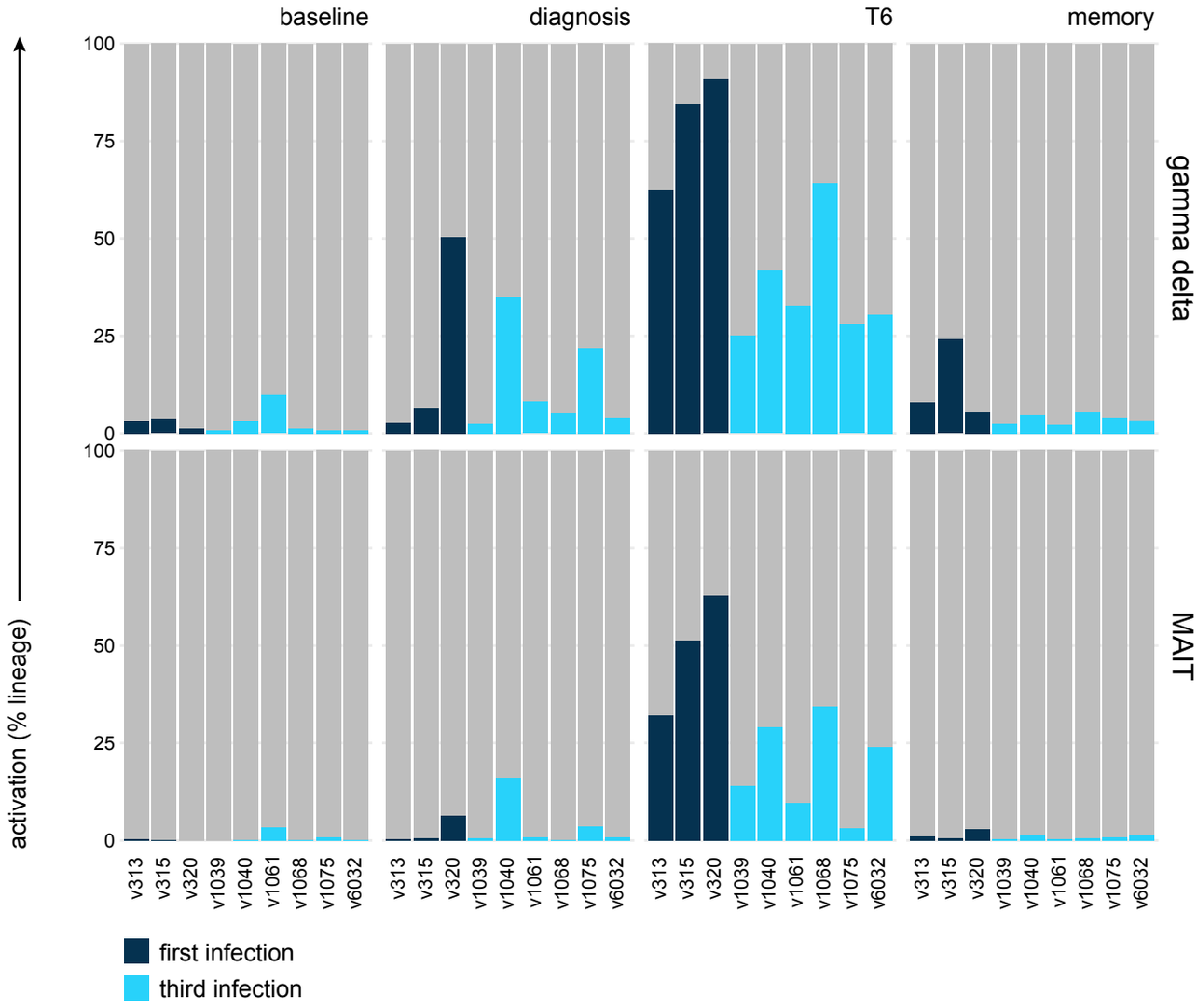

figure five - supplement 6

Figure 5 - supplement 6 | Innate-like T cells are highly activated in tolerised hosts. Bar charts display the frequency of activated ($CD38^{hi}$ $Bcl2^{lo}$) gamma delta and MAIT clusters at each time-point. Data are shown as a proportion of the entire lineage ($V\delta2^{pos}$ for gamma delta and $V\alpha7.2^{pos}$ for MAIT). n = 3 (first infection) and 6 (third infection).

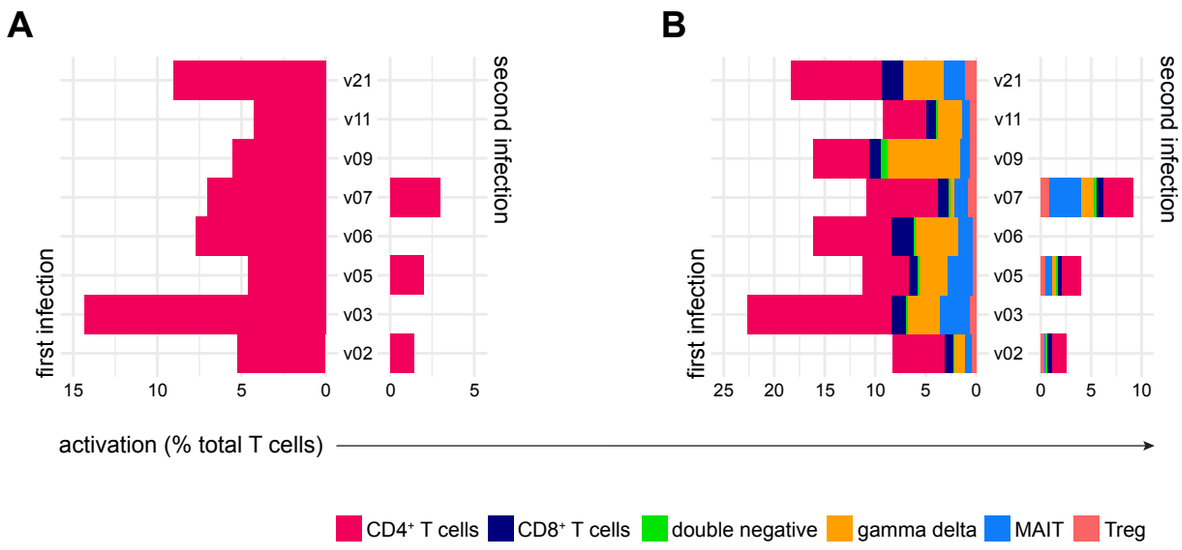

figure six - supplement 1

Figure 6 - supplement 1 | *Plasmodium vivax* induces tolerance after a single infection. Six healthy malaria-naive adults were infected with *P. vivax* (clone PvW1) by direct blood challenge and three volunteers returned for a homologous re-challenge 8-months later. These CHMI trials were called VAC069A and VAC069B, respectively. Two additional healthy malaria-naive volunteers were infected with PvW1 (for the first time) during VAC069B. In both trials, whole blood was preserved within 30-minutes of blood draw at baseline, diagnosis and 6-days post-treatment (T6) - samples were stained with a T cell focussed antibody panel and acquired on a Helios mass cytometer. After exclusion of normalisation beads and doublets we gated on $CD45^{pos}$ $CD3^{pos}$ T cells for FlowSOM clustering, which was performed independently for VAC069A and VAC069B. (**A**) Bar chart showing the frequency of activated ($CD38^{hi}$ $Bcl2^{lo}$) $CD4^{+}$ T cell clusters at T6. (**B**) Stacked bar chart showing the frequency of all activated ($CD38^{hi}$ $Bcl2^{lo}$) T cell clusters at T6. In (A-B) data are shown as a proportion of all $CD45^{pos}$ $CD3^{pos}$ T cells and n = 8 (first infection) or 3 (second infection).

948 Supplementary files

949 **Supplementary file 1** | Demographics of volunteers infected and re-challenged with *Plasmodium*
950 *falciparium* (3D7); includes genetic and non-genetic variables known to influence human immune
951 variation *in vitro*. Also shown is the parasite multiplication rate (detailed methodology for the
952 modelling of qPCR data can be found in Minassian *et al*. (47)) and maximum core body temperature
953 measured in each volunteer during each infection. There were no statistically significant differences
954 between first, second and third infection (Kruskal-Wallis test, $p = 0.3287$ for parasite multiplication
955 rate and $p = 0.9949$ for core temperature).

956 **Supplementary file 2** | Pearson correlation coefficient and p value measuring the relationship
957 between inflammation, coagulation, symptoms, parasites and T cell activation. These data underpin
958 the matrix shown in figure 3C.

959 **Supplementary file 3** | Mass cytometry antibody panel for T cell fate and function in falciparum
960 malaria; includes information on antibody clone and heavy metal conjugate.

961 References

962 1. B. P. Goncalves *et al.*, Parasite burden and severity of malaria in Tanzanian children. *N Engl*
963 *J Med* **370**, 1799-1808 (2014).
964 2. C. A. Moxon, M. P. Gibbins, D. McGuinness, D. A. Milner, Jr., M. Marti, New Insights into
965 Malaria Pathogenesis. *Annu Rev Pathol* **15**, 315-343 (2020).
966 3. R. W. Snow, K. Marsh, New insights into the epidemiology of malaria relevant for disease
967 control. *Br Med Bull* **54**, 293-309 (1998).
968 4. R. W. Snow *et al.*, Risk of severe malaria among African infants: direct evidence of clinical
969 protection during early infancy. *J Infect Dis* **177**, 819-822 (1998).
970 5. D. L. Doolan, C. Dobano, J. K. Baird, Acquired immunity to malaria. *Clin Microbiol Rev* **22**,
971 13-36 (2009).
972 6. J. Tuju *et al.*, Antigenic cartography of immune responses to Plasmodium falciparum
973 erythrocyte membrane protein 1 (PfEMP1). *PLoS Pathog* **15**, e1007870 (2019).
974 7. K. Cumnock *et al.*, Host Energy Source Is Important for Disease Tolerance to Malaria. *Curr*
975 *Biol* **28**, 1635-1642 e1633 (2018).
976 8. S. Ramos *et al.*, Renal control of disease tolerance to malaria. *Proc Natl Acad Sci U S A* **116**,
977 5681-5686 (2019).
978 9. A. Wang *et al.*, Glucose metabolism mediates disease tolerance in cerebral malaria. *Proc*
979 *Natl Acad Sci U S A* **115**, 11042-11047 (2018).
980 10. R. Medzhitov, D. S. Schneider, M. P. Soares, Disease tolerance as a defense strategy.
981 *Science* **335**, 936-941 (2012).
982 11. T. W. Ademolue, Y. Aniweh, K. A. Kusi, G. A. Awandare, Patterns of inflammatory responses
983 and parasite tolerance vary with malaria transmission intensity. *Malar J* **16**, 145 (2017).
984 12. W. Nahrendorf, A. Ivens, P. J. Spence, Inducible mechanisms of disease tolerance provide
985 an alternative strategy of acquired immunity to malaria. *Elife* **10**, (2021).
986 13. K. Milne *et al.*, Mapping immune variation and var gene switching in naive hosts infected with
987 Plasmodium falciparum. *Elife* **10**, (2021).
988 14. D. I. Stanisic, J. S. McCarthy, M. F. Good, Controlled Human Malaria Infection: Applications,
989 Advances, and Challenges. *Infect Immun* **86**, (2018).
990 15. J. K. Baird *et al.*, Adult Javanese migrants to Indonesian Papua at high risk of severe disease
991 caused by malaria. *Epidemiol Infect* **131**, 791-797 (2003).
992 16. J. K. Baird *et al.*, Age-dependent susceptibility to severe disease with primary exposure to
993 Plasmodium falciparum. *J Infect Dis* **178**, 592-595 (1998).
994 17. S. J. Draper *et al.*, Malaria Vaccines: Recent Advances and New Horizons. *Cell Host Microbe*
995 **24**, 43-56 (2018).
996 18. C. J. Duncan, S. J. Draper, Controlled human blood stage malaria infection: current status
997 and potential applications. *Am J Trop Med Hyg* **86**, 561-565 (2012).
998 19. Q. Cheng *et al.*, Measurement of Plasmodium falciparum growth rates in vivo: a test of
999 malaria vaccines. *Am J Trop Med Hyg* **57**, 495-500 (1997).
1000 20. P. J. Spence *et al.*, Vector transmission regulates immune control of Plasmodium virulence.
1001 *Nature* **498**, 228-231 (2013).
1002 21. E. Spaulding *et al.*, STING-Licensed Macrophages Prime Type I IFN Production by
1003 Plasmacytoid Dendritic Cells in the Bone Marrow during Severe Plasmodium yoelii Malaria.
1004 *PLoS Pathog* **12**, e1005975 (2016).

1005 22. D. Ghosh, J. S. Stumhofer, The spleen: "epicenter" in malaria infection and immunity. *J*
1006 *Leukoc Biol*, (2021).
1007 23. C. F. Ockenhouse *et al.*, Common and divergent immune response signaling pathways
1008 discovered in peripheral blood mononuclear cell gene expression patterns in presymptomatic
1009 and clinically apparent malaria. *Infect Immun* **74**, 5561-5573 (2006).
1010 24. T. M. Tran *et al.*, Transcriptomic evidence for modulation of host inflammatory responses
1011 during febrile Plasmodium falciparum malaria. *Sci Rep* **6**, 31291 (2016).
1012 25. L. Hviid *et al.*, Rapid reemergence of T cells into peripheral circulation following treatment of
1013 severe and uncomplicated Plasmodium falciparum malaria. *Infect Immun* **65**, 4090-4093
1014 (1997).
1015 26. V. H. Carpio *et al.*, T Helper Plasticity Is Orchestrated by STAT3, Bcl6, and Blimp-1 Balancing
1016 Pathology and Protection in Malaria. *iScience* **23**, 101310 (2020).
1017 27. M. A. Koch *et al.*, The transcription factor T-bet controls regulatory T cell homeostasis and
1018 function during type 1 inflammation. *Nat Immunol* **10**, 595-602 (2009).
1019 28. C. Y. Fonseka *et al.*, Mixed-effects association of single cells identifies an expanded effector
1020 CD4(+) T cell subset in rheumatoid arthritis. *Sci Transl Med* **10**, (2018).
1021 29. H. Mattoo *et al.*, Clonal expansion of CD4(+) cytotoxic T lymphocytes in patients with IgG4-
1022 related disease. *J Allergy Clin Immunol* **138**, 825-838 (2016).
1023 30. K. Marsh, R. W. Snow, Host-parasite interaction and morbidity in malaria endemic areas.
1024 *Philos Trans R Soc Lond B Biol Sci* **352**, 1385-1394 (1997).
1025 31. G. Napolitani *et al.*, Clonal analysis of Salmonella-specific effector T cells reveals serovar-
1026 specific and cross-reactive T cell responses. *Nat Immunol* **19**, 742-754 (2018).
1027 32. M. F. Chughlay *et al.*, Liver Enzyme Elevations in Plasmodium falciparum Volunteer Infection
1028 Studies: Findings and Recommendations. *Am J Trop Med Hyg* **103**, 378-393 (2020).
1029 33. I. J. Reuling *et al.*, Liver Injury in Uncomplicated Malaria is an Overlooked Phenomenon: An
1030 Observational Study. *EBioMedicine* **36**, 131-139 (2018).
1031 34. J. Woodford, G. D. Shanks, P. Griffin, S. Chalon, J. S. McCarthy, The Dynamics of Liver
1032 Function Test Abnormalities after Malaria Infection: A Retrospective Observational Study.
1033 *Am J Trop Med Hyg* **98**, 1113-1119 (2018).
1034 35. M. Dudek *et al.*, Auto-aggressive CXCR6(+) CD8 T cells cause liver immune pathology in
1035 NASH. *Nature* **592**, 444-449 (2021).
1036 36. S. Gupta, R. W. Snow, C. A. Donnelly, K. Marsh, C. Newbold, Immunity to non-cerebral
1037 severe malaria is acquired after one or two infections. *Nat Med* **5**, 340-343 (1999).
1038 37. R. S. Osii, T. D. Otto, P. Garside, F. M. Ndungu, J. M. Brewer, The Impact of Malaria
1039 Parasites on Dendritic Cell-T Cell Interaction. *Front Immunol* **11**, 1597 (2020).
1040 38. J. Kim *et al.*, Innate-like Cytotoxic Function of Bystander-Activated CD8(+) T Cells Is
1041 Associated with Liver Injury in Acute Hepatitis A. *Immunity* **48**, 161-173 e165 (2018).
1042 39. N. P. Weng, K. Liu, M. Catalfamo, Y. Li, P. A. Henkart, IL-15 is a growth factor and an
1043 activator of CD8 memory T cells. *Ann N Y Acad Sci* **975**, 46-56 (2002).
1044 40. R. M. Welsh, L. K. Selin, No one is naive: the significance of heterologous T-cell immunity.
1045 *Nat Rev Immunol* **2**, 417-426 (2002).
1046 41. B. M. Greenwood, Possible role of a B-cell mitogen in hypergammaglobulinaemia in malaria
1047 and trypanosomiasis. *Lancet* **1**, 435-436 (1974).
1048 42. L. C. Mourao, G. P. Cardoso-Oliveira, E. M. Braga, Autoantibodies and Malaria: Where We
1049 Stand? Insights Into Pathogenesis and Protection. *Front Cell Infect Microbiol* **10**, 262 (2020).

1050 43. L. Deng, R. A. Mariuzza, Recognition of self-peptide-MHC complexes by autoimmune T-cell
1051 receptors. *Trends Biochem Sci* **32**, 500-508 (2007).
1052 44. N. L. Smith *et al.*, A Conserved TCRbeta Signature Dominates a Highly Polyclonal T-Cell
1053 Expansion During the Acute Phase of a Murine Malaria Infection. *Front Immunol* **11**, 587756
1054 (2020).
1055 45. N. Malaria Genomic Epidemiology, Insights into malaria susceptibility using genome-wide
1056 data on 17,000 individuals from Africa, Asia and Oceania. *Nat Commun* **10**, 5732 (2019).
1057 46. E. Patin *et al.*, Natural variation in the parameters of innate immune cells is preferentially
1058 driven by genetic factors. *Nat Immunol* **19**, 302-314 (2018).
1059 47. A. M. Minassian *et al.*, Reduced blood-stage malaria growth and immune correlates in
1060 humans following RH5 vaccination. *Med (N Y)* **2**, 701-719 (2021).
1061 48. R. O. Payne *et al.*, Demonstration of the Blood-Stage Plasmodium falciparum Controlled
1062 Human Malaria Infection Model to Assess Efficacy of the P. falciparum Apical Membrane
1063 Antigen 1 Vaccine, FMP2.1/AS01. *J Infect Dis* **213**, 1743-1751 (2016).
1064 49. B. Langmead, S. L. Salzberg, Fast gapped-read alignment with Bowtie 2. *Nat Methods* **9**,
1065 357-359 (2012).
1066 50. C. A. Harrington *et al.*, RNA-Seq of human whole blood: Evaluation of globin RNA depletion
1067 on Ribo-Zero library method. *Sci Rep* **10**, 6271 (2020).
1068 51. H. Shin *et al.*, Variation in RNA-Seq transcriptome profiles of peripheral whole blood from
1069 healthy individuals with and without globin depletion. *PLoS One* **9**, e91041 (2014).
1070 52. M. I. Love, W. Huber, S. Anders, Moderated estimation of fold change and dispersion for
1071 RNA-seq data with DESeq2. *Genome Biol* **15**, 550 (2014).
1072 53. H. Wickam, ggplot2: Elegant Graphics for Data Analysis. *Springer-Verlag New York*, (2016).
1073 54. H. Mizuno, Y. Nakanishi, N. Ishii, A. Sarai, K. Kitada, A signature-based method for indexing
1074 cell cycle phase distribution from microarray profiles. *BMC Genomics* **10**, 137 (2009).
1075 55. J. Pena-Diaz *et al.*, Transcription profiling during the cell cycle shows that a subset of
1076 Polycomb-targeted genes is upregulated during DNA replication. *Nucleic Acids Res* **41**,
1077 2846-2856 (2013).
1078 56. D. Dominguez *et al.*, A high-resolution transcriptome map of cell cycle reveals novel
1079 connections between periodic genes and cancer. *Cell Res* **26**, 946-962 (2016).
1080 57. B. Giotti, A. Joshi, T. C. Freeman, Meta-analysis reveals conserved cell cycle transcriptional
1081 network across multiple human cell types. *BMC Genomics* **18**, 30 (2017).
1082 58. P. Chomczynski, N. Sacchi, The single-step method of RNA isolation by acid guanidinium
1083 thiocyanate-phenol-chloroform extraction: twenty-something years on. *Nat Protoc* **1**, 581-585
1084 (2006).
1085 59. G. Bindea *et al.*, ClueGO: a Cytoscape plug-in to decipher functionally grouped gene
1086 ontology and pathway annotation networks. *Bioinformatics* **25**, 1091-1093 (2009).
1087 60. B. Mlecnik *et al.*, Functional network pipeline reveals genetic determinants associated with
1088 in situ lymphocyte proliferation and survival of cancer patients. *Sci Transl Med* **6**, 228ra237
1089 (2014).
1090 61. R. Finck *et al.*, Normalization of mass cytometry data with bead standards. *Cytometry A* **83**,
1091 483-494 (2013).
1092 62. E. R. Zunder *et al.*, Palladium-based mass tag cell barcoding with a doublet-filtering scheme
1093 and single-cell deconvolution algorithm. *Nat Protoc* **10**, 316-333 (2015).
1094 63. H. Crowell, V. Zanotelli, S. Chevrier, M. Robinson, CATALYST: Cytometry dATa anALYSis
1095 Tools. *R/Bioconductor* **version 1.14.0**, (2020).

1096 64. S. Chevrier *et al.*, Compensation of Signal Spillover in Suspension and Imaging Mass
1097 Cytometry. *Cell Syst* **6**, 612-620 e615 (2018).
1098 65. L. McInnes, J. Healy, J. Melville, UMAP: Uniform Manifold Approximation and Projection for
1099 Dimension Reduction. *arXiv:1802.03426*, (2020).
1100 66. D. J. McCarthy, K. R. Campbell, A. T. Lun, Q. F. Wills, Scater: pre-processing, quality control,
1101 normalization and visualization of single-cell RNA-seq data in R. *Bioinformatics* **33**, 1179-
1102 1186 (2017).
1103 67. S. Van Gassen *et al.*, FlowSOM: Using self-organizing maps for visualization and
1104 interpretation of cytometry data. *Cytometry A* **87**, 636-645 (2015).
1105 68. Y. Saeys, S. Van Gassen, B. Lambrecht, Response to Orlova et al. "Science not art:
1106 statistically sound methods for identifying subsets in multi-dimensional flow and mass
1107 cytometry data sets". *Nat Rev Immunol* **18**, 78 (2017).
1108 69. Z. Gu, R. Eils, M. Schlesner, Complex heatmaps reveal patterns and correlations in
1109 multidimensional genomic data. *Bioinformatics* **32**, 2847-2849 (2016).
1110 70. M. Nowicka *et al.*, CyTOF workflow: differential discovery in high-throughput high-
1111 dimensional cytometry datasets. *F1000Res* **6**, 748 (2017).
1112 71. L. M. Weber, M. Nowicka, C. Soneson, M. D. Robinson, diffcyt: Differential discovery in high-
1113 dimensional cytometry via high-resolution clustering. *Commun Biol* **2**, 183 (2019).
1114 72. M. D. Robinson, D. J. McCarthy, G. K. Smyth, edgeR: a Bioconductor package for differential
1115 expression analysis of digital gene expression data. *Bioinformatics* **26**, 139-140 (2010).